International Journal for Multidisciplinary Research (IJFMR)
E-ISSN: 2582-2160 ● Website: www.ijfmr.com ● Email: editor@ijfmr.com

Doping Effects of Pigment Oxides on Optical and Mechanical Properties of PbO-Based Glasses

Debajyoti Mahapatra[1], Subrata Panda[2], Anil Kumar[3], Preetam Singh[4]

[1,2,3,4]Department of ceramic engineering, IIT (BHU), Varanasi- 221005, Uttar Pradesh, India

Abstract

The current academic study focuses on analysis and synthesization of a high density, high refractive indexed heavy metal oxide pigmented heat absorbent sodium silicate glass system xPbO-y(0.14Cu_2O-0.05CuO-0.03SnO_2) -30Na_2O-(70-0.22y-x)SiO_2 (x= 0,1.5,10 mol% and y = 0,1) explored with various ratios PbO doping via conventional melt annealing route, resulted optimally suited material for various linear and nonlinear optoelectronic applications. The fundamental physio-mechanical properties like density(ρ), molar volume(V_m), and oxygen packing density (OPD) of synthesized samples were analysed, alongside elastic moduli were computed utilizing experimental, Makishima-Mackenzie, & Rocherulle models. When the XRD data verified the substance's amorphous character, the FTIR study specified the vibrational bands associated with the silicate matrix's structure. The visible optical properties, solar optical properties, refractive index (n), extinction coefficient (k) optical dielectric constants, direct &indirect optical band gap, and Urbach energy (E_U) were measured from computed spectral data collected by Jasco V-770 spectrophotometer in the solar spectrum wavelength spanning 190 nm - 1100 nm, as a result, the computed indirect optical band gap energy (E_{gind}) and, direct optical band gap energy (E_{gd}) were illustrated to be in the 1.64-2.61 and, 2.57-3.03 eV range respectively. Using the absorption spectra, the average of refraction index (n_0), corresponding nonlinear refractive index (n_2), molar refraction (R_m), polarizability (α_m), reflection loss (R_L), optical transmission (T), metallization criterion (M_c), optical electronegativity ($\Delta\chi^*$), third order nonlinear optical susceptibility($\chi^{(3)}$) have all been calculated, whereas the beneficiary parameter, optical basicity (Λ_{th}) has been also evaluated. All the above characterizations have been established and explored, paving the road for the created product to be an acceptable option for commercial construction, especially for exterior use in high-light areas as well as optoelectronic devices.

Keywords: Pigmented high-density glass; X-Ray; UV-Visible; FTIR

1. Introduction

Silicate glasses are the most popular commercially available glasses having high viscosity, which facilitates glass formation without crystallization [1]. Multiple kinds of silicate glasses have numerous uses for building creation, decorative industries, electronic devices, radioactive and photovoltaic tools, acoustic-optic devices etc. because of their outstanding thermal resilience, thermo-mechanical properties, and chemical-based strength [2-3], and in optics for telecommunication applications due to their excellent transmission and low attenuation losses in the apparent and near-IR zones[4]. Silicate glasses have become more prevalent in commercial and residential buildings for their excellent ability to capture and transmit

visible daylight into buildings [5]. Pure silicate glass forms noticeably clear glass having high transmission properties compared to other building coverings, and along with consequently, becoming the main provider of extra solar radiation inside the building, making the building residents unpleasant. However, this problem has been solved by doping specific amounts of transition metals or rare earth ions into silicate glasses making the glasses tinted and heat-absorbing without compromising their strength, which reduces and controls the significant amount of solar radiation transmission into the buildings.

Among the transition metals, the valence configuration of copper in glasses influences not only the physical and chemical features yet its capability to create glasses [6]. The outstanding brilliant sharp blue-green colour glass is produced because of the existence of Cu^{2+} ions according to ligand field theory [7]. The copper atom's electronic configuration is [Ar] $3d^{10}4s^{1}$, including two persistent ion states, Cu^{+} and Cu^{2+}. Due to entirely occupied five d-orbital cuprous ion (Cu^{+}) does not produce colouring [8], but Cu^{2+} ion produces a colour centre featuring bands of absorption in the visible-light area and creates interesting bluish occasionally green colour in material [9]. It has been studied that the intensity of colouring based on Cu^{2+} concentration, and its coordination, including the alkalinity of glasses [8,9]. Present-day Cu^{2+} ion-doped glasses are the most popular research area due to their optical bistability [7,10].

Besides doping with transition metals or rare earth ions, incorporating suitable proportions for heavy metallic oxides makes the glasses more useful. It has been observed that adding heavy metal oxides (BaO, Bi_2O_3, PbO, etc.) into the glasses improved some unique properties of glasses such as chemical resilience, refractive index, density, improving ability to resist devitrification, & reducing processing temp [11]. Moreover, the heavy metal oxide silicate glasses have high values of the mass attenuation coefficients and excellent shielding properties against nuclear radiations [12,13]. Many previous researchers observed that silicate glasses containing suitable amounts of heavy metal oxides showed enhanced linear and nonlinear optical properties [14], excellent infrared transmission [15], and low crystallization tendency [16]. These multicomponent glasses with PbO have a broad application in enamels, optics such as lenses for optics, ultrasonic delay cables, electro-optic modulators, electro-optic toggles, solid-state laser resources, electrons boosts, television image tubes, and other related important optical electronic uses and glass-to-metal sealing due to their low processing temperatures, high resistance to devitrification, high chemical durability, high optical density, and refractive index [17-19]. Such spectacles can also be useful in additional scientific purposes like upconverting phosphors, mechatronics, dosimetry, radiation physics, along with waveguides for light since they have low phonon energy [20,21], along with specific uses in a certain field for heated as well as mechanical detectors, low-loss fibre optics as well infrared-transmitting components [22]. The molecular significance of Pb^{2+} in silica glass is currently being thoroughly investigated to show its fascinating function during glass creation in multiple structures, especially silicon dioxide [23-31]. Earlier authors showed that in binary lead silicate glasses, Pb functions to be a glassmaker with a significant lead amount as well as an interconnected enhancer for a small amount of lead [32]. PbO is not able to form a glass matrix on its own, but when mixed in suitable amounts with other glass-forming oxides like SiO_2, B_2O_3, TeO_2, and P_2O_5, it can create glass [33], and generate an ionic or covalent bond between oxygen [34].

Besides transition metal ions and heavy metal oxides, it has been found that incorporating suitable amounts of SnO_2 in silicate glass structure improved the compactness of the tinted glass which significantly facilitated the glass composition to be used against high photon energies [35]. Earlier researchers also noticed that appropriate doping of SnO_2 in their glass composition upgraded the glass photosensitivity, microhardness, and thermal stability [36,37]. Ziemath et al. claimed that Sn^{4+} cations in their glass

composition worked like an interconnected former leading to more rigid glass development, by using the UV-visible absorbance & scattered reflection examination within the infrared spectrum [38]. One disadvantage of SnO_2 is that larger concentrations cause the opacity of silicate glass due to its limited solubility within the silica network [39], making it unwanted when the glass is used as a building construction material. Nevertheless, the above literature survey shows that incorporating a very little and controlled amount of Sn^{4+}, Cu^{2+}, Cu^{+}, and Pb^{2+} ions in a soda silicate glass improves the glass properties which may be suitable for widespread applications in various fields.

Motivated by the above literature survey, this research work primarily focused on the development of PbO-based tint glasses with improved optical and mechanical properties for widespread applications. The other obvious objective was to optimize the PbO contents in the tint glass compositions for optimum physical, optical, and mechanical properties for building construction materials. A range of characterization techniques were employed to explore glass interconnection structures, which might be causally related via the improved physical, optical, mechanical, and optoelectronic properties of the examined tint glasses.

2. Experimental procedures

2.1. Preparation of tint glasses

A sodium silicate base glass ($30Na_2O$-$70SiO_2$) was used to prepare a range of tint glass compositions and the corresponding compositions are given in **Table 1**. A general formula can be expressed as $xPbO$-$y(0.14Cu_2O$-$0.05CuO$-$0.03SnO_2)$-$30Na_2O$-$(70-0.22y-x)SiO_2$ (x = 0,1.5,10 mol% and y = 0,1) for all the prepared compositions. High-purity reagent grade cuprous oxide (Cu_2O, 97% freshness), copper monoxide (CuO, 97% freshness) supplied through Avarice Industries, and lead oxide (PbO, 99.99% purity) supplied by Aldrich Chemical Co. were used as sources of Cu_2O, CuO, and PbO, respectively. Tin oxide (SnO_2, 98% purity), sodium carbonate (Na_2CO_3, 99% purity), and quartz (SiO_2, 99% freshness) supplied through Loba Chemie were served as sources of SnO_2, Na_2O, and SiO_2, respectively. All the respective batch compositions were weighted by utilizing an electronic micro analytical weighing machine having a precision of ± 0.0001 g, afterwards blended by using a high- powered ball mill (Amaze Instruments) at 400 rpm for 2 h for obtaining a homogeneous batch mixture. Each batch mixture was taken in the aluminium crucible for glass melting in an electric furnace at about 1400 °C during 6 h as per the melting profile as shown in **Fig. 1(a)**. The molten glass was poured over a preheated alumina plate before chilling, pulverizing, later remelting around similar time-temperature profile to produce extra uniform glass formation. The remelted glass was finally poured onto a preheated iron mold having specific dimensions for obtaining rectangular samples. The readied rectangular fragments were annealed at 500 °C during 4 h by using a fixed time-temperature profile as illustrated in **Fig. 1(b)** to prevent them from shattering due to internal residual stresses.

Table 1. Molar compositions of the prepared glasses and their respective batch compositions (wt.%).

Glass samples	Molar glass compositions	Batch compositions (wt.%)					
		Cu_2O	CuO	SnO_2	PbO	Na_2O	SiO_2
Base Glass	$(Na_2O)_{30}(SiO_2)_{70}$	-	-	-	-	30.70	69.30

S1	$(PbO)_{1.50}(Na_2O)_{30}(SiO_2)_{68.50}$	-	-	-	5.31	29.50	65.19
S2	$(PbO)_{10}(Na_2O)_{30}(SiO_2)_{60}$	-	-	-	29.01	24.18	46.80
S3	$(Cu_2O)_{0.14}(CuO)_{0.05}(SnO_2)_{0.03}(Na_2O)_{30}(SiO_2)_{69.78}$	0.329	0.0654	0.074	-	30.61	68.91
S4	$(Cu_2O)_{0.14}(CuO)_{0.05}(SnO_2)_{0.03}(PbO)_{1.50}(Na_2O)_{30}(SiO_2)_{68.28}$	0.316	0.0628	0.071	5.29	29.42	64.82
S5	$(Cu_2O)_{0.14}(CuO)_{0.05}(SnO_2)_{0.03}(PbO)_{10}(Na_2O)_{30}(SiO_2)_{59.78}$	0.259	0.0515	0.058	28.95	24.132	46.53

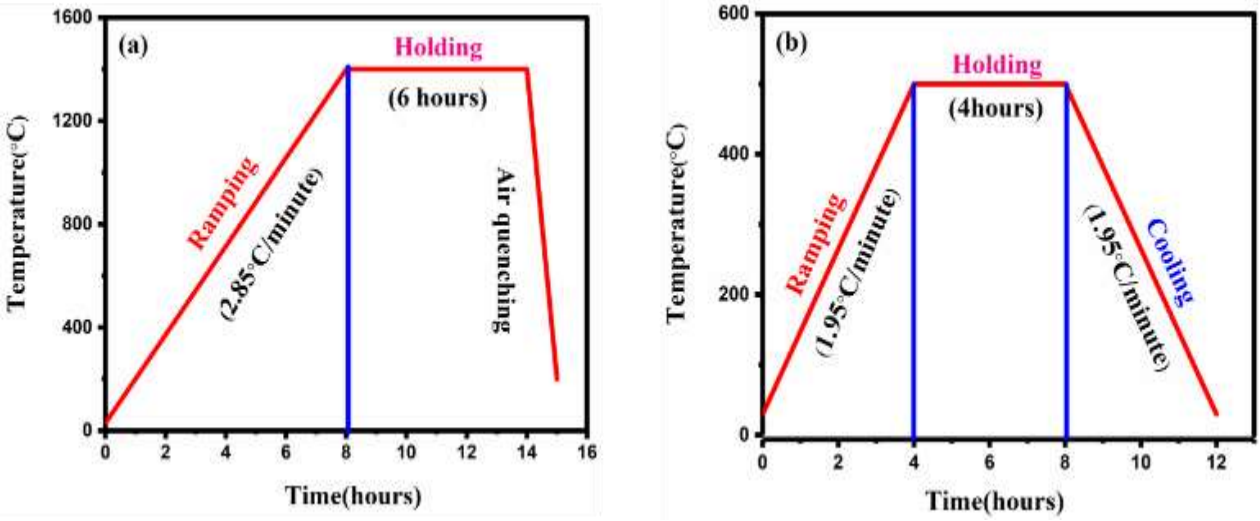

Fig. 1. (a) Time-temperature profile for the melt-quenching process, and (b) time-temperature profile for the annealing process.

2.2 Materials Characterizations

Density of the prepared tint glasses was ascertained during ambient temperature applying the law of Archimedes where water was utilized as the dipping liquid. The overall density assessment had an estimated deviation of about ± 0.004 g cm^{-3}. The prepared glasses' molar volume was determined by using the formula ($V_m = M/\rho$, where V_m is the molar volume, M is the molar mass and ρ is the density of the glass). The oxygen packing density (OPD) of the glass specimens was deduced applying the formula, $OPD = (1000 \times k \times \rho)/M$, wherein the number of oxygen atoms per mole in a composition is denoted by k, ρ is the density of the glass, and M is the molecular weight of the glass [40].

Each bulk glass sample was shaped and polished employing 400/800/1200 water-cooled silicon carbide (SiC) dusts & 6/3/1/0.025 µm diamond paste followed by mechanical cutting using a water-cooled low-speed diamond saw. All the determined attempts were done to secure that each side of the samples is aligned to each other having a fluctuation of below 0.05 cm and obtain maximum flatness of the sample surfaces. The photographs of the polished glass samples for optical characterization are shown in **Fig. 2**. The optically polished glasses' ultraviolet and visible spectrum were captured employing Jasco V-770 double beam UV-VIS spectrophotometer (Japan) connected with PC UV-Win lab software, where the visible and solar optical characteristics of the pigmented glasses were determined by taking a weighted

average of the experimental data over 360 nm to 830 nm. The data was gathered at 5 nm intervals considering the normal incidence of light in the ultraviolet and entire visible spectral zones, which comprises transmission in the specular transmission mode, reflection in the diffuse reflection mode, and absorption in the spectrum mode. The weighted factors for evaluating solar optical characteristics were taken in a US standard atmosphere containing 3.4 mm of ozone and 20 mm of precipitable H_2O vapor, normally in sunshiny atmosphere [41]. The Lambert-Bear equation $\left(I_t = I_O e^{-\alpha(\omega)d}\right)$ was employed to calculate the materials absorption coefficient $\alpha(\omega)$ for each glass at different photon energies $\hbar(\omega)$, wherein d is the sample thickness and I_O and I_t is the incident and transmitted photon intensities, correspondingly.

Fig. 2. Photographs of optically polished glass samples prepared for optical characterization.

All the synthesized tint glasses were pulverized into fine powders by mortar pestle for executing XRD analysis at room temperature. The fine powder was taken in a sample holder in Ragaku Smart Lab (9 KW) powder type X-ray diffraction apparatus of RIGAKU Corporation company (Japan) equipped with graphite monochromatic copper Kα radiation source (λ = 1.540 Å) and Ni filter tube ran at 40 kV & 20 mA current. All the XRD data were recorded throughout a span of 2θ from 10º to 80º using a scan rate of 3º min^{-1} and all the sets of data were interpreted by applying PANalytical XPert High Score along with correlating using standard ICDD (International Center for Diffraction Data) cards. Infrared spectra of all the glass powder samples were analyzed throughout wavenumbers (4000-450 cm^{-1}) at 4 cm^{-1} clarity in transmittance mode for illuminating functional groups that exist in the glasses. All the data were measured on a single-beam Nicolet iS5 FTIR spectrometer of THERMO Electron Scientific Instruments LLC Company (USA) at room temperature utilizing the KBr disc technique.

The longitudinal (V_L) along with shear (V_S) ultrasonic wave velocities were calculated in an ambient temperature by utilizing an ultrasonic flaw detector machine, in which two quartz X- and Y-cut transducers are functioning at 5 MHz resonant frequency having an error of ± 10 m/s ambiguity.

3. Results and discussion

3.1 Physical properties of the tint glasses

It has been found that all produced glasses are transparent. In the respective oxide glass systems, {xPbO-y(0.14Cu_2O-0.05CuO-0.03SnO_2) -30Na_2O-(70-0.22y-x) SiO_2} authors denoted the composition of glass systems y(0), and y(1), when y=0, and y=1 correspondingly in the respective glass composition. OPD is a key parameter that describes the framework of glass & assesses the rigidity of the oxide system. All the produced glass samples' OPD values are found between 57.331 & 71.86 mol/liter. The density, molar volume, & OPD data are presented in **Table 2**. The values indicate that increasing concentration of PbO (0≤x≤10, x in mol%) and the addition of metallic oxides (<0.22mol%) (Cu_2O+CuO+SnO_2) in sodium silicate glass systems decrease OPD which shows the development of NBOs in the glass latticework, resulting more loosely packed network structure.

3.2 XRD analysis

The XRD spectrum of synthesized glass samples with different compositions and base glass which are all listed in **Table 1** are displayed in **Fig. 3**. The spectra spanning the region of 2θ, 10° to 80° of all glass samples depict no distinct peaks indicating the irregular character of entire synthesized glass specimens due to the decided trace amount of doped ingredients and have been detected with a predominant initial hump in all the glass samples XRD data's due to the base glass as provided in a previous research paper [42].

Table 2. Density, molar volume, & oxygen packing density of the created coloured glasses.

Samples	Thickness (cm)	Density (g/cm^3)	Molar volume (cm^3/mol.)	Oxygen packing density (OPD)
S1	0.796	2.689	23.446	71.86
S2	0.81	3.190	24.113	66.35
S3	0.801	2.491	24.389	69.63
S4	0.806	2.5856	22.471	68.85
S5	0.802	2.765	27.874	57.33

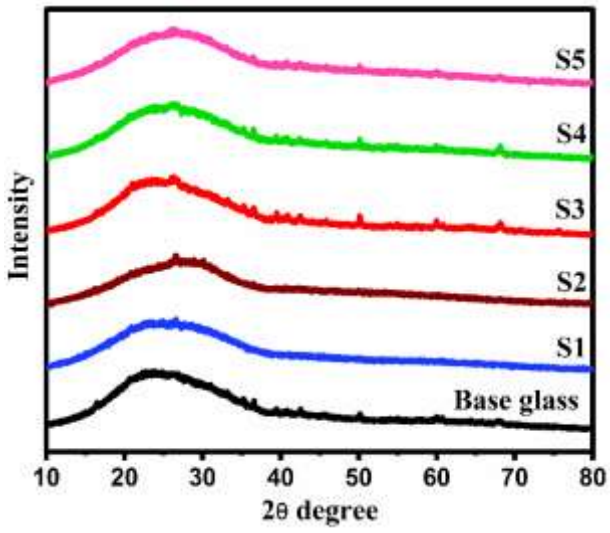

Fig. 3. XRD curves of all-synthesized glass samples.

3.3 FTIR Spectroscopy

The obtained FTIR spectral measurements of base glass and other all doped tint glasses with different compositions provided in **Table 1** are displayed in **Fig. 4**. The infrared spectrum reveals two different distinct areas in the 500 - 4000 cm^{-1} range. The distinctive vibrational bands, the majority that can be found in the smaller spectral region, are allocated to the IR spectral fingerprint region, although the functional group area, which showed in the larger spectral region, is crucial for identifying the sample's fundamental characteristics. Two moderately clear infrared bands develop around adjacent to 460 cm^{-1} &

783 cm^{-1} respectively, a considerably deep infrared wideband is observed on nearly 1038 cm^{-1}, two tiny dim infrared bands are detected at around 1384 cm^{-1} & 1625 cm^{-1} and a strong infrared wideband is seen at about 3440 cm^{-1}. The extensive broadband at roughly 1038 cm^{-1} in all the glass samples' FTIR spectra appeared because of uneven stretching vibration of the Si-O bond in the SiO_4 tetrahedron groups that exist in the silicate phases of the glass specimens [43,44]. A further moderately wide band on nearly 460 cm^{-1} in all the FTIR glass samples data are obtained due to the bending vibrations of O-Si-O bond in the SiO_4 tetrahedron groups present in the glass samples and vibrations of metallic cations such as Pb^{2+} [45,46]. The attributed assignments of all the transmission peaks in all the glass samples' FTIR data sets are given in **Table 3**. No significant changes are observed in all the FTIR glass samples data and hence it is concluded that the determined amounts of metallic concentrations (Cu_2O+CuO+SnO_2), and PbO have shown no considerable influence on the silicate network structure.

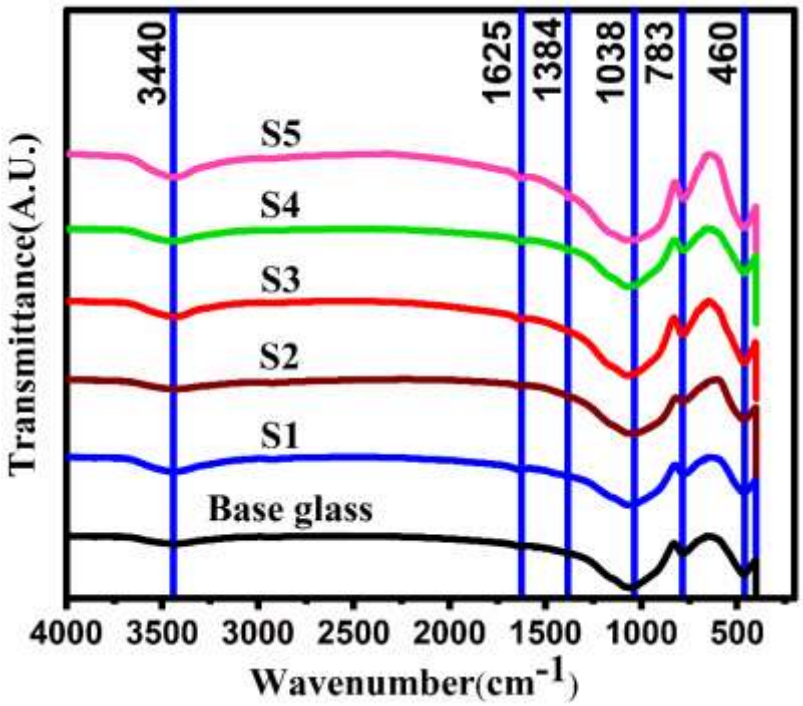

Fig. 4. All prepared glass specimens' FTIR spectrum having compositions xPbO-y(0.14Cu_2O-0.05CuO-0.03SnO_2) -30Na_2O-(70-0.22y-x) SiO_2 (for S1, S2, S3, S4, S5, (x,y) = (1.5,0), (10,0), (0,1),(1.5,1), (10,1) respectively).

Table 3. FTIR spectrum allocations of all prepared glass compositions.

Wavenumber (cm^{-1})	Bonding	Sources
460	Bending vibrations of O-Si-O bonds in SiO_4 tetrahedral groups including oscillations of metal cations such as Pb^{2+}	[45,46]
783	Due to the bending of conjugated SiO_4 tetrahedral groups and oxygen atoms connected perpendicularly to the Si-Si axis within the Si-O-Si plane, in the SiO_2 glass network structure.	[45,47, 48]
1038	Uneven stretching of the O-Si-O bond within the SiO_4 tetrahedral group.	[43,44]

1384	Due to the antisymmetric vibrations of oxygen atoms connected to Si-O-Si groups	[43]
1625	Due to the vibration of the H_2O molecule and symmetric stretching of O-H bonds	[43,47]
3440	Associated with the stretching of the (OH) group and molecular water.	[42]

3.4 UV-VIS Spectroscopy

The spectral reflection and transmission in the visible region and absorbance in the ultraviolet and visible region of respective rectangular optical polished glass samples (S1, S2, S3, S4, &S5) having thicknesses between 7.96 to 8.10 mm with different compositions (**Table 1**) are shown in **Fig. 5**. The measured reflections of the colored glass samples S1, S2, S3, S4, and S5 exhibit its highest intensity band in the visible range about 830 nm, 528 nm, 528 nm, 497 nm, and 484 nm, respectively (**Fig. 5a**). Similarly, the acquired transparency of the glass samples S1, S2, S3, S4, and S5 reveal their maximum peak in the visible range of about 830 nm, 530 nm, 531 nm, 488nm, and 491 nm respectively (**Fig. 5b**).

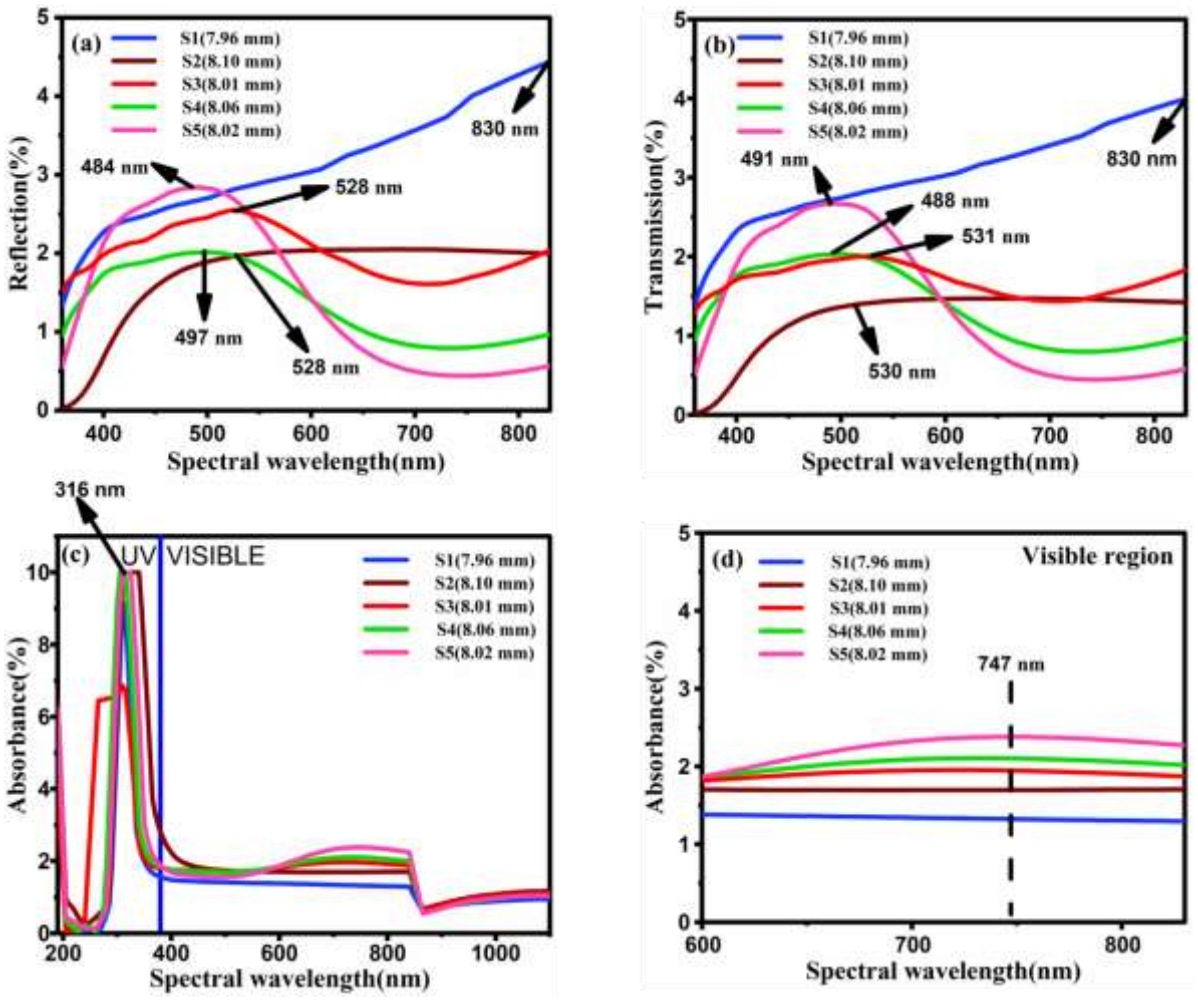

Fig. 5. Spectral reflections (a) in the visible region, spectral transmissions(b) in the visible region, and spectral absorbance(c) in the ultraviolet and visible region and spectral absorbance(d)in the wavelength range of 600 to 830 nm in the visible region respectively.

3.4.1 Visible Optical Properties

The reflectance, transmittance, and absorbance of selected samples (S1, S2, S3, S4, & S5) spanning the visible light wavelength of 360 nm to 830 nm are measured experimentally applying ISO standards [49], as well as the weighted mean of visible optical characteristics are calculated using the Eq. (1), Eq. (2), and Eq. (3) which are provided bellow.

$$T_{VIS} = \frac{\sum_{\lambda=360nm}^{\lambda=830nm} D_\lambda \tau(\lambda) v(\lambda) \Delta\lambda}{\sum_{\lambda=360nm}^{\lambda=830nm} D_\lambda v(\lambda) \Delta\lambda} \quad (1)$$

$$R_{VIS} = \frac{\sum_{\lambda=360nm}^{\lambda=830nm} D_\lambda \mu(\lambda) v(\lambda) \Delta\lambda}{\sum_{\lambda=360nm}^{\lambda=830nm} D_\lambda v(\lambda) \Delta\lambda} \quad (2)$$

$$A_{VIS} = 100 - T_{VIS} - R_{VIS} \quad (3)$$

Where $\Delta\lambda$ is wavelength intervals, D_λ is the relative spectral distribution of illuminant D65, $v(\lambda)$ is spectral luminous efficiency for the field of view vision deciding the average observer for spectrophotometric study, $\tau(\lambda)$ is spectral transmittance (%), $\mu(\lambda)$ is spectral reflectance (%) while a correlation (Eq. (3)) provided the absorption from glass specimens over the visible region.

All the measured visible optical properties of all glass samples obtained by using a UV-VIS spectrophotometer are provided in **Table 4**. The mentioned visible characteristics are essential when assessing daylighting into houses.

Table 4. Visible optical parameter, solar optical parameter, indirect and direct optical band gap and, Urbach energy of all prepared glass samples.

Sample	Visible optical properties			Solar optical properties			E_{gind} (eV)	E_{gd} (eV)	E_U (eV)
	T_{VIS} (%)	R_{VIS} (%)	A_{VIS} (%)	T_{solar} (%)	R_{solar} (%)	A_{solar} (%)			
S1	40	40	20	40	41	19	2.61	3.03	0.0640
S2	27	38	35	27	37	36	2.42	2.86	0.0642
S3	31	39	30	30	36	34	1.90	2.80	0.0596
S4	33	32	35	28	28	44	1.85	2.60	0.0683
S5	34	36	30	28	29	43	1.64	2.57	0.0684

3.4.2 Solar Optical Properties

The solar optical characteristics of selected glass specimens in the complete visible spectrum wavelength between 360 nm to 830 nm employing British along with ISO standards are assessed by the Eq. (4), Eq. (5), and Eq. (6) provided bellow [5].

$$T_{solar} = \frac{\sum_{\lambda=360nm}^{\lambda=830nm} S_\lambda \tau(\lambda) \Delta\lambda}{\sum_{\lambda=360nm}^{\lambda=830nm} S_\lambda \Delta\lambda} \quad (4)$$

$$R_{solar} = \frac{\sum_{\lambda=360nm}^{\lambda=830nm} S_\lambda \mu(\lambda) \Delta\lambda}{\sum_{\lambda=360nm}^{\lambda=830nm} S_\lambda \Delta\lambda} \quad (5)$$

$$A_{solar} = 100 - T_{solar} - R_{solar} \quad (6)$$

Where, S_λ is the relative spectral distribution of the solar radiation (W/m^2), whereas relationship (Eq. (6)) gives solar absorbance. Solar optical properties have a significant impact on heating & cooling burdens, that enhance building power usage. These properties are essential in assessing heat load in dwellings across windowpanes and are provided in **Table 4**.

3.4.3 Refractive index (n) and extinction coefficient (k)

The real component of the complex refractive index is the index of refraction (n), which is connected to the reflection function (R) and the extinction coefficient (k) as per Fresnel theory which is provided in Eq. (7).

$$R = \frac{(n-1)^2+k^2}{(n+1)^2+k^2} \quad (7)$$

The algorithms mentioned in Eq. (8), and Eq. (9) are employed to compute the refractive indexes of entire synthesized glass specimens having various compositions.

$$T_s = 10^{-A} \times 100 \quad (8)$$

$$n = \frac{1}{T_s} + \sqrt{\frac{1}{(T_s-1)}} \quad (9)$$

Where, T_s denotes per cent transmittance or per cent transmittance constant, while A represents absorbance. The extinction coefficient (k) is determined by implementing the Eq. (10).

$$k = \frac{\alpha\lambda}{4\pi} \quad (10)$$

wherein α & λ signify for materials' absorption coefficient and wavelength correspondingly.

Connecting and quasi anions and cations in the Ultraviolet region, as well as grid oscillations in glass networking in the infrared region, are two dominant transmission aspects which influence glass system's refractive index [50]. The dispersion curves of refractive indexes and extinction coefficients for all five prepared glass specimens are illustrated in **Fig. 6** and **Fig. 7**, which present that the refractive index (n), and extinction coefficient (k) improve within ultraviolet, and visible area with the addition of the respective determined amount of metal oxides (Cu_2O+CuO+SnO_2), and PbO (**Table 1**) in the glass composition.

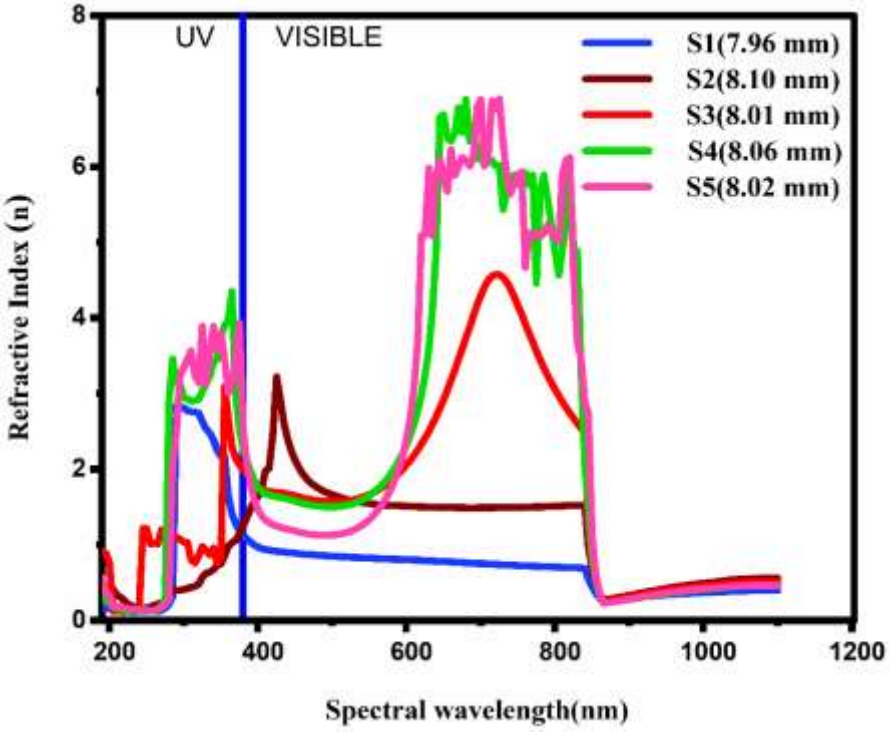

Fig. 6. The distribution plot of refractive index (n) vs wavelength of all prepared glass specimens.

3.4.4 Complex dielectric constant

The optical complex dielectric constant, that is determined by molecular mechanisms originating from

photon interactions with electrons, is indeed a factor of refractive index n and extinction coefficient k. The complex dielectric constants contain real and imaginary components, designated by $\mathcal{E}_r(\mathcal{E}_r = n^2 + k^2)$, and $\mathcal{E}_i(\mathcal{E}_i = 2nk)$ [50]. The dispersion curves for the real component of the complex dielectric constant $(\mathcal{E}_r)$ as well as the exponent of the complex dielectric constant $(\mathcal{E}_i)$ of all five glass samples are depicted in **Fig. 8**, which becomes evident that both parts {real $(\mathcal{E}_r)$, & imaginary$(\mathcal{E}_i)$} of the complex dielectric constant develop highly within ultraviolet, and visible area with the addition of the respective determined amount of metal oxides (**Table 1**) inside sodium silicate glass structure.

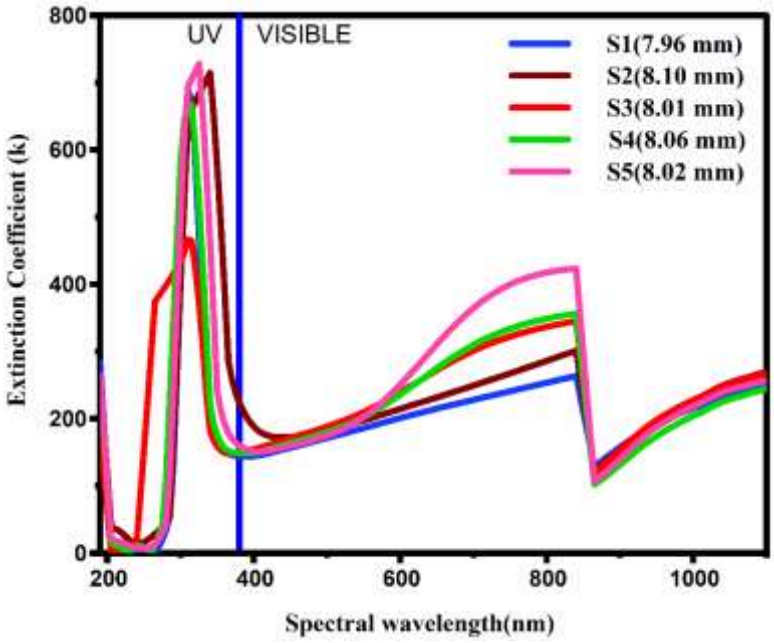

Fig. 7. The distribution plot of extinction coefficient (k) vs wavelength of entire prepared glass specimens.

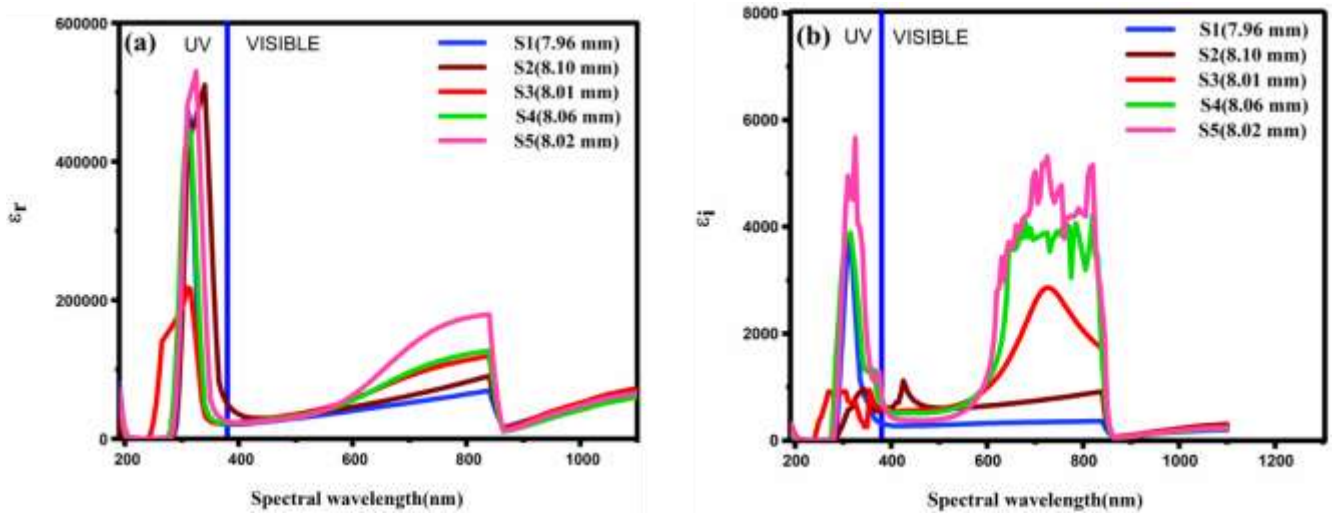

Fig. 8. Illustration of the dispersion plot of the real part of the complex dielectric constant $(\mathcal{E}_r)$ along with the imaginary part of the complex dielectric constant $(\mathcal{E}_i)$ respectively with the wavelength of prepared glass specimens.

3.4.5 Assessment of the optical energy gap

The Tauc's plot of five similar optical polished glass specimens with nearly equal thicknesses but varying compositions for both indirect & direct transition are provided in **Fig. 9** and **Fig. 10** respectively. The Davis and Mott formula (Eq. (11)) is applied to estimate the energy gap of the synthesized samples [50].

$$(\alpha hv) = B\left(hv - E_g\right)^r \quad (11)$$

Where, B is a constant, E_g is an optical energy gap, h is a plank constant, and r is an index number having values of 1/2, 2, 3/2, and 1/3 according to the electronic transition pathway. Usually, the values of r for permitted electronic transitions are 1/2 for direct transition and 2 for indirect transition. For all five glass samples with varying compositions, the tauc's plot is constructed among $(\alpha hv)^{1/r}$ on the ordinate with photon energy (hv) on the abscissa to assess the optical band gap. The optical band gaps are determined using the tauc's graph curve's linear section by inference at $(\alpha hv)^r = 0$ (where, r=0.5 for indirect transition and r=2 for direct transition). The optical energy gap results for all five glass specimens are provided in **Table 4** when the optical energy gap values of pure $30Na_2O$-$70SiO_2$ glass are obtained from prior author research articles [51]. **Fig. 11** shows that the resulting optical energy gap (indirect, & direct) of the y(1) glass series shows a significantly reduce amount than y(1) glass series, and both in the glass series the optical energy gap (indirect, & direct) reduce with the addition of respective amounts of PbO (0≤x≤10, x in mol%).

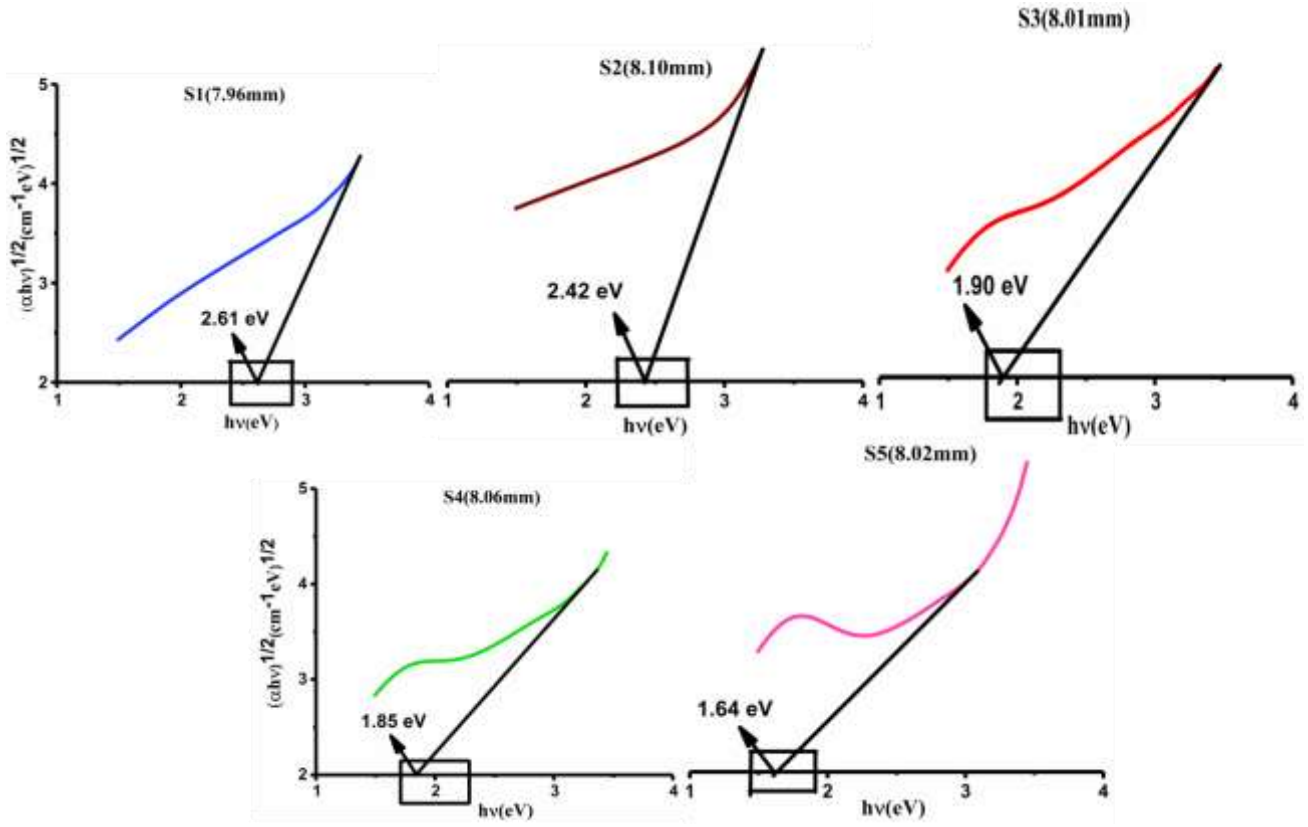

Fig. 9. Tauc's plot of specified samples contains indirect transitions.

3.4.6 Evaluation of molar refraction (R_m), polarizability (α_m), reflection loss (R_L), optical transmission (T), and metallization criterion (M_c), by using refractive index (n_0) calculated by Tauc's technique.

The degree of total polarizability for each unit mole is defined by the substance's molar refraction (R_m). The molar refraction of synthesized glass specimen is evaluated by the following Lorentz–Lorenz equation Eq. (15) [52].

$$R_m = \left(\frac{n_0^2-1}{n_0^2+2}\right) V_m \quad (12)$$

where, the refractive index (n_0) is calculated by the Eq. (13) while the achieved values are presented in **Table 5**. The (n_0) ranges (2.51-2.91) are regarded as significant and evolve as the addition of the determined amount of metallic concentration (<0.22mol%) (Cu_2O+CuO+SnO_2), and increasing PbO (0≤x≤10, x in mol%) concentration in the studied glass system. As an outcome, the glasses under review can be employed as effective prospects for a wide range of optical purposes.

$$\left(\frac{n_0^2-1}{n_0^2+2}\right) = 1 - \sqrt{\frac{E_g}{20}} \quad (13)$$

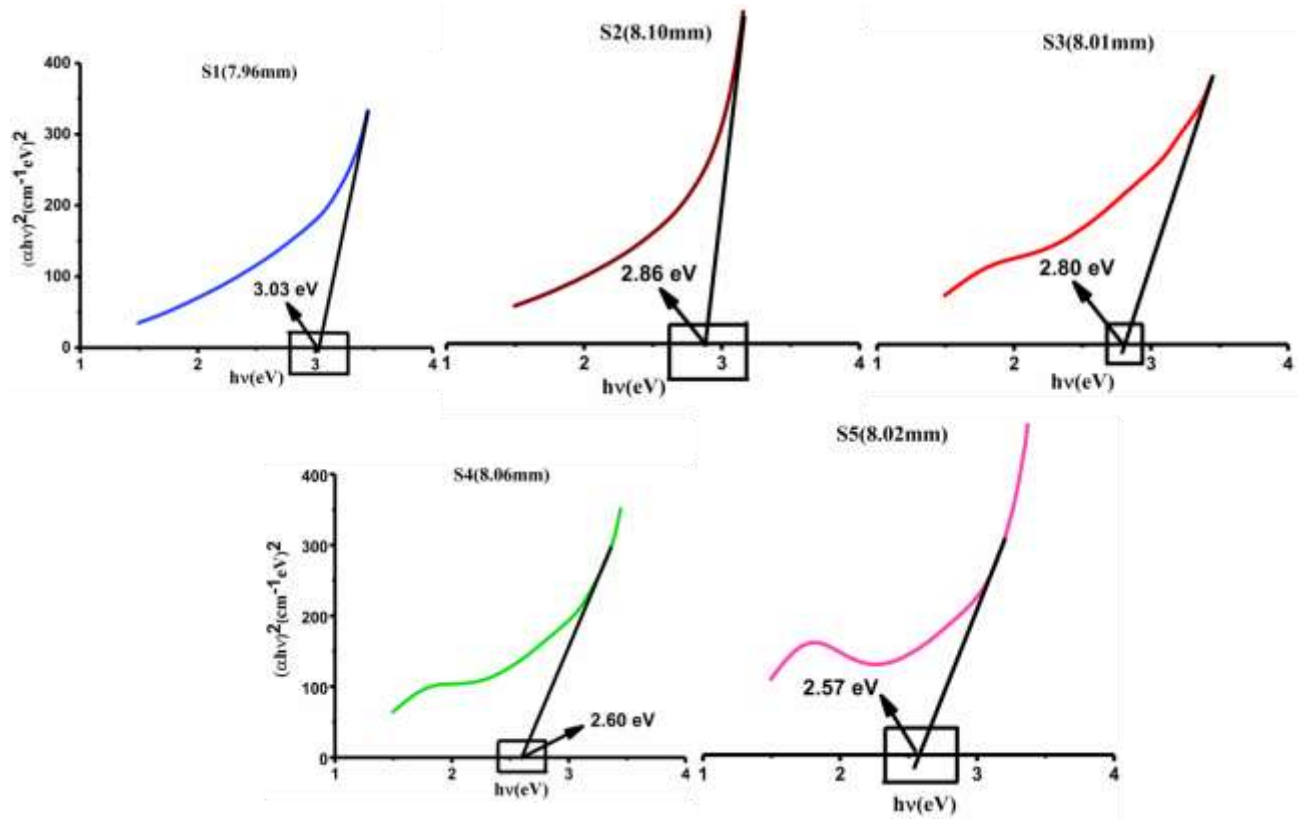

Fig. 10. Tauc's plot of specified samples contains direct transitions.

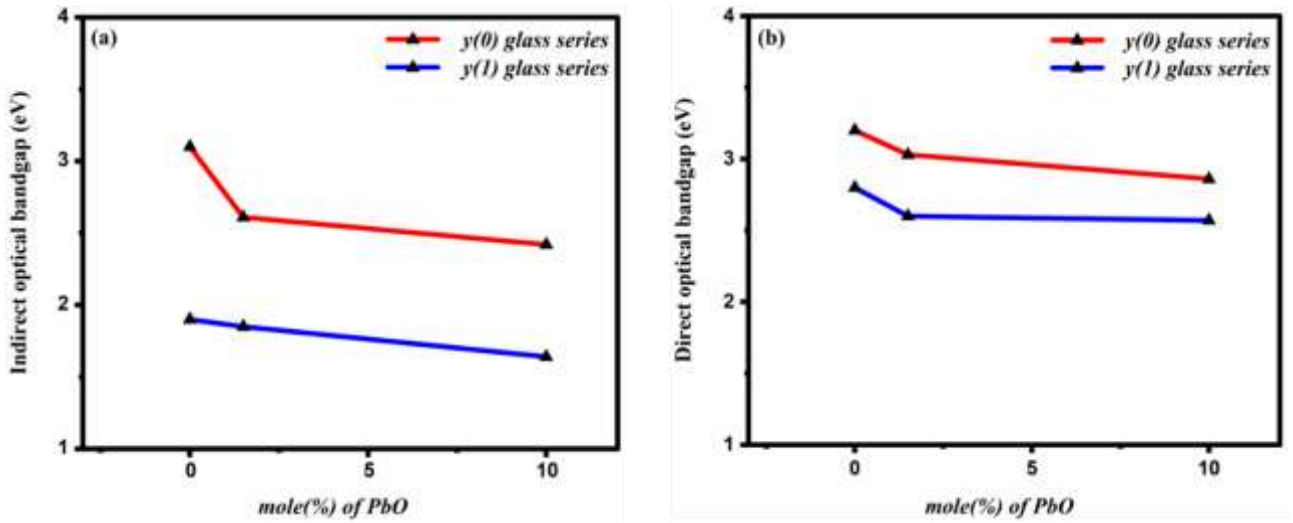

Fig. 11. depict the influence of indirect, and direct optical energy gaps respectively with the addition of PbO (0≤x≤10, x in mol%) in the examined glass system {xPbO-y(0.14Cu_2O-0.05CuO-0.03SnO_2) -30Na_2O-(70-0.22y-x) SiO_2}.

Table 5. Calculated refractive index (n_0) adopting Tauc's method and, corresponding nonlinear refractive index $(n_2) \times 10^{-13}$ for the studied glass specimens.

Sample code	S1	S2	S3	S4	S5
Calculated refractive index (n_0) via Tauc's method	2.51	2.57	2.78	2.80	2.91
Corresponding nonlinear refractive index $(n_2) \times 10^{-13}$ (esu)	8.09	9.88	18.97	20.12	27.51

The amplitude of electrons interacting with an electric field is determined by a molecule's electronic polarizability (α_m), and this can be defined as a function of molar refraction as used in Eq. (14) [52]:

$$\alpha_m = \left(\frac{R_m}{2.52}\right) \quad (14)$$

The (R_L) and (T) values of the produced glass specimens were determined by Eq. (15), and (16) respectively.

$$R_L = \left(\frac{n_0-1}{n_0+1}\right)^2 \quad (15)$$

$$T = \left(\frac{2n_0}{n_0^2+1}\right) \quad (16)$$

The metallization criterion factor (M_c) determines if a material is metallic or insulator. The (M_c) values of entire synthesized glass specimens are computed through Eq. (17).

$$M_c = 1 - \left(\frac{R_m}{V_m}\right) \quad (17)$$

The (R_m),(α_m),(R_L), (T), (M_c) values of entire produced glass specimens are depicted through the bar graph of **Fig. 12(a)**, **Fig. 12(b)**, **Fig. 12(c)**, **Fig. 12(d)**, and **Fig. 12(e)** respectively. As obtained (R_m) values of these developed glasses are less than their (V_m) values respectively, we may deduce that the prepared glasses are non-metallic (insulators) [52].

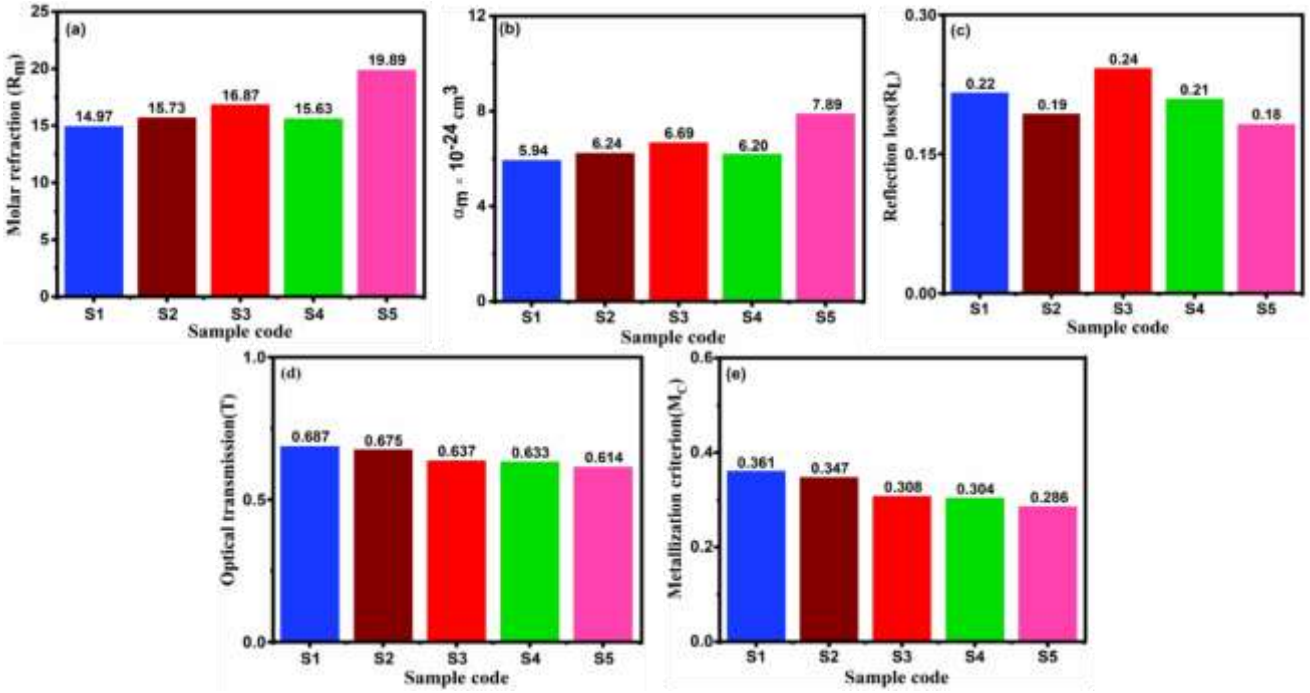

Fig. 12. Bar graph of studied samples contains calculated molar refraction (R_m)(Fig. 12(a)), polarizability(α_m)(Fig. 12(b)), reflection loss (R_L) (Fig. 12(c)), optical transmission(T)(Fig. 12(d)) and, metallization criterion (M_c) (Fig. 12(e)).

3.4.7 Assessment of optical electronegativity $(\Delta\chi^*)$, third order nonlinear optical susceptibility $(\chi^{(3)})$, and associated nonlinear refractive index (n_2) employing refractive index (n_0) computed by Tauc's approach.

The optical electronegativity $(\Delta\chi^*)$ indicates the type of bonding in the samples [53]. The high and low $(\Delta\chi^*)$ value specifies ionic and covalent bonding respectively. The $(\Delta\chi^*)$ value of all the prepared samples is determined through Eq. (18)

$$\Delta\chi^* = 0.2688\,(E_g) \tag{18}$$

The obtained values of $(\Delta\chi^*)$ are illustrated through the bar graph of **Fig. 13(a)**, while the calculated $(\Delta\chi^*)$ values are judged poor, so the bonding characteristic of the prepared specimens may be classified as covalent bonding. The third-order nonlinear optical susceptibility $(\chi^{(3)})$ in the esu unit of the examined glasses is assessed by using the Eq. (19), while the obtained values $(\chi^{(3)})$ of entire examined glass specimens are depicted through the bar graph of **Fig. 13(b)**. It is clearly noticed that $(\Delta\chi^*)$, & $(\chi^{(3)})$ values reduce and enhance respectively due to the addition of a determined amount of metallic oxide (<0.22mol%) (Cu_2O+CuO+SnO_2), and the increasing amount of PbO (0≤x≤10, x in mol%) concentration in the investigated glass systems.

$$\chi^{(3)}\,(esu) = \frac{A}{(4\pi)^4}\,(n_0^2 - 1)^4 \tag{19}$$

in which A is fixed and approximately 1.7 ×10^{10}. The nonlinear refractive indexes (n_2) for all selected glasses are computed through the following Eq. (20) and listed in **Table 5**.

$$n_2(esu) = \frac{12\pi\chi^{(3)}}{n_0} \tag{20}$$

The outcomes indicate that (n_2) alters with the addition of metallic oxides (<0.22mol%) (Cu_2O+CuO+SnO_2), and PbO (0≤x≤10, x in mol%) inside sodium silicate glass structure and linked to the amount of non-bridging oxygen (NBO) within respective glass species.

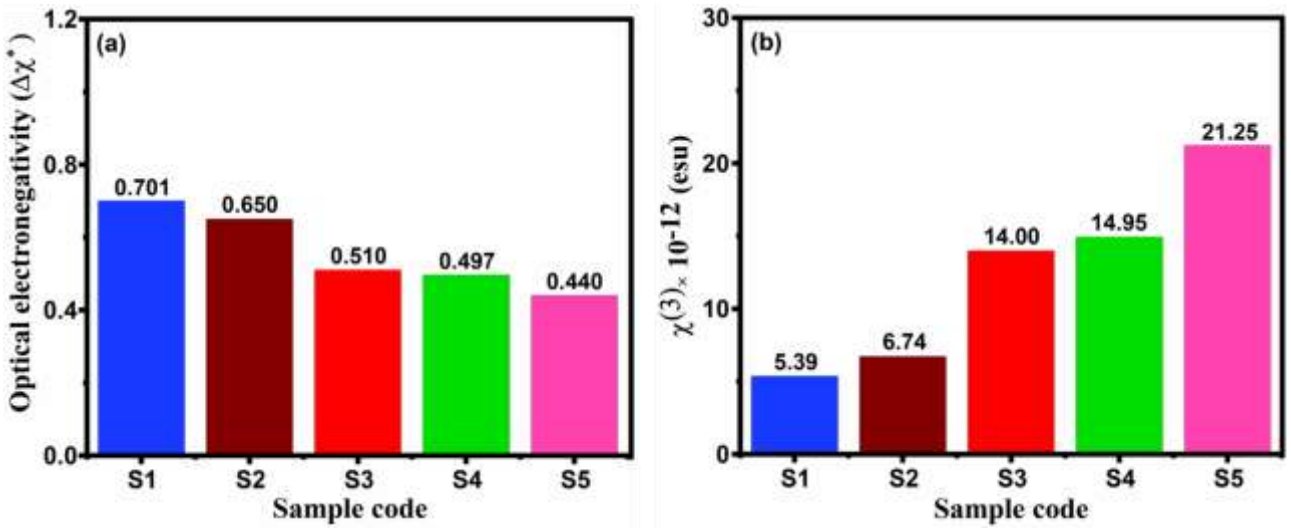

Fig. 13. Bar graph of studied samples contains calculated optical electronegativity $(\Delta\chi^*)$(Fig. 13(a)) as well as third-order nonlinear optical susceptibility $(\chi^{(3)})$ (Fig. 13(b)).

3.4.8 Measurement of the Urbach energy

Urbach energy has been employed to assess energetic disorder at a semiconductor or insulator's band borders and is only faintly influenced by temperature. The weak crystalline and chaotic amorphous materials contain proximal states that are stretched in the band gap and generated as band ends in the conventional band gap. The Urbach empirical rule defines the absorption coefficient (α) as a function of photon energy (hv) in the poor photon energy domain. The Urbach empirical rule is presented in Eq. (21).

$$\alpha = \alpha_0 \, exp\left(\frac{hv}{E_U}\right) \quad (21)$$

where, α_0 and E_U denote constant and band tail energy or Urbach energy respectively. Considering the logarithms of both sides of Eq. (22), we obtain

$$ln(\alpha) = ln(\alpha_0) + \left(\frac{hv}{E_U}\right) \quad (22)$$

As a result, $E_U = \frac{1}{m}$, wherein m represents the gradient of a straight line derived by graphing $ln(\alpha)$ versus incident photon energy (hv). The graph of $ln(\alpha)$ vs incoming photon energy (hv) of prepared samples with varying compositions is provided in **Fig. 14** to calculate the Urbach energy of every specimen. The Urbach value fluctuates between 0.0596 to 0.0684 eV for the glass specimens in the investigation (as shown in **Table 4**). The Urbach energy rises as the metallic concentrations (<10.22 mol%) (Cu_2O+CuO+SnO_2+ PbO) of the glass grow, implying that the defect concentrations in the glass matrix additionally develop.

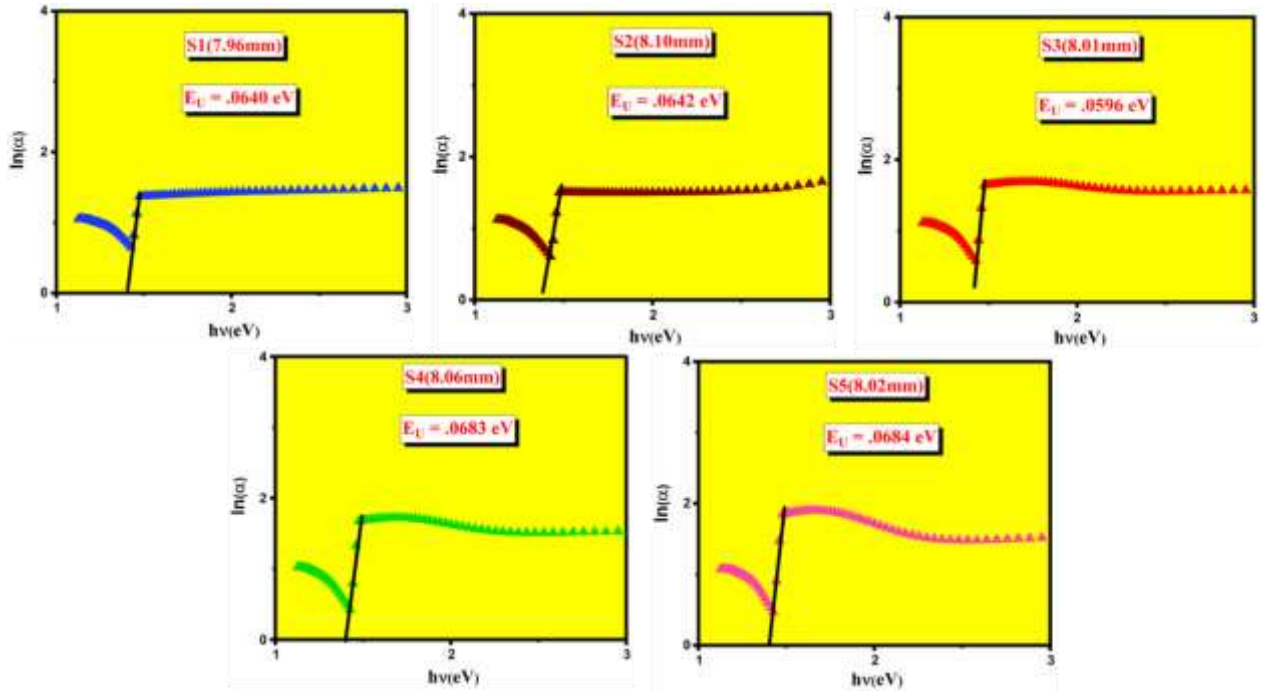

Fig. 14. The graph of $ln(\alpha)$ against incident photon energy $(h\nu)$ of studied specimens.

3.4.9 Analysis of UV-Vis's absorption edges

The absorbance spectrum of prepared glass samples is primarily influenced by parent glass composition, melting temperature, duration of the melting process, partial pressure of oxygen throughout melting, annealing temperature, rate of cooling, additionally, the background losses (reflection loss, absorbance caused by OH groups, IR edge, etc.) detected in the absorbance spectra due to dopants, refining compounds, other absorbent impurities [54]. The resulting absorption assessment of the concerned largely metallic doped glass specimens (S3, S4, S5) reveals its maximum absorbance of around 747 nm in the visible area (**Fig. 5(d)**), and all the glass specimens show its maximum absorbance of around 316 nm in the UV region (**Fig. 5(c)**). At conventional melting circumstances, in the currently prepared glass samples (S3, S4, S5) the metallic element copper appears in the form of Cu^{2+} ions while some of it exists as Cu^{0} and Cu_2O [55-58]. Previously, researchers found the absorption band caused by Cu^{2+} ions at 786 nm in silicate glasses, 1048 nm in aluminoborophosphate glasses, and 1390 nm in sodium aluminoborate glasses [59-63]. The currently prepared glass samples (S3, S4, S5) containing Cu_2O, CuO exhibit a growing single broad absorption band from 600 nm to 830 nm (**Fig. 5(d)**), which is very conceivable related to the assignment of an electronic transition of one of the ingredient's cupric ions. The obtained rising band might be generated by the electronic transition from $^{2}\mathbf{E_g} \rightarrow {}^{2}\mathbf{T_g}$ energy level in octahedral coordination of Cu^{2+} ion, implying a distorted octahedral symmetry for cupric ion in the current S3, S4, S5 glass samples [63,64]. The all-glass samples (S1,S2,S3,S4,S5) exhibit a high charge transfer ultraviolet absorption band around 316 nm which may be caused by iron impurities as well as the contribution of Pb^{2+} ions present in the all-respective glass samples [65].

3.5 Optical basicity of the tint glasses (Λ_{th})

The optical basicity parameter (Λ) can be utilized to categorize an assortment of oxidic glasses according to their basicity order and implies oxide glass's capacity to produce a negative charge to the probing ion [66,67]. It relates characteristics like refractive index independently of the anionic configuration of the

glass under concern [66]. Duffy and Ingram stated that the optical basicity of glass might be expected by considering its composition and proposed the Eq. (23) to compute this parameter [67].

$$\Lambda_{th} = \sum_i X_i \Lambda_i \quad (23)$$

Where, X_i is the equivalent fraction determined by the quantity of oxygen given by each oxide to the total glass stoichiometry and Λ_i is the basicity attributed to the respective oxide [68,69]. The basicity moderating parameter (γ_i) is determined by applying the Eq. (24) [70].

$$\gamma_i = 1.36(x_i - 26) \quad (24)$$

Wherein x_i is the cation's Pauling electronegativity. The optical basicity (Λ_{th}) of the prepared glasses is examined and reported through the bar graph of **Fig. 15**. All cations available in the glass matrices and their Pauling electronegativity (x_i), optical basicity moderating parameter (γ_i), and optical basicity (Λ) are listed below in **Table 6**. The measurements of optical basicity (Λ_{th}) rise from 0.5986 to 0.6508, as the addition of metallic oxides (<0.22mol%) (Cu_2O+CuO+SnO_2), and PbO (0≤x≤10, x in mol%) concentration rises, caused by expanding electrons on oxygen atoms [69].

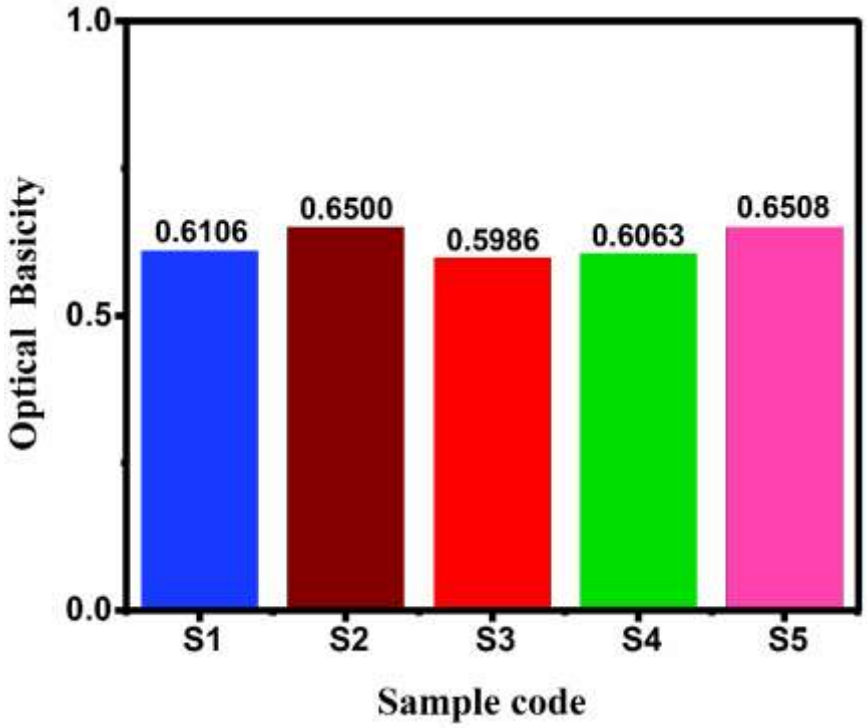

Fig. 15. Bar graph of investigated samples contains calculated optical basicity.

Table 6. Glass basicity characteristics

Cation	Pauling electronegativity (x_i)	Basicity moderating parameter (γ_i)	$(\Lambda) = \frac{0.75}{(x_i - 0.25)}$	$(\Lambda) = [\gamma_i]^{-1}$
Pb	2.33	2.8152	0.360576923	0.35521455
Na	0.93	0.9112	1.102941176	1.097453907

Si	1.9	2.2304	0.454545455	0.448350072
Cu	1.9	2.2304	0.454545455	0.448350072
Sn	1.96	2.312	0.438596491	0.432525952

3.6 Mechanical properties

The longitudinal (L_m), shear (G_m), bulk(k_m), Young's(E_m)modulus, hardness(H), and Poisson's ratio (υ) of the respective tint glasses were calculated by employing the measured longitudinal ultrasonic velocity (V_L), and shear ultrasonic velocity (V_S) and the corresponding values are given in **Table 7** [71]. The formulas used for determining the mechanical properties are provided bellow.

$$L_m = \rho V_L^2 \quad (25)$$

$$G_m = \rho V_s^2 \quad (26)$$

$$k_m = L_m - \left(\frac{4}{3}\right) G_m \quad (27)$$

$$E_m = \frac{9k_m G_m}{3k_m + G_m} \quad (28)$$

$$H = \frac{(1-2\upsilon)E_m}{6(1+\upsilon)} \quad (29)$$

$$\upsilon = \frac{E_m}{2G_m} - 1 \quad (30)$$

Table 7. Mechanical properties of the tint glasses

Samples	V_L (m/s)	V_S (m/s)	L_m (GPa)	G_m (GPa)	k_m (Gpa)	E_m (Gpa)	H (GPa)	υ
S1	5954.77	3609.83	95.35	35.04	48.63	84.76	6.78	0.2095
S2	5134.98	3200.22	84.11	32.67	40.55	77.26	6.91	0.1824
S3	6118.72	3761.77	93.26	35.25	46.26	84.33	7.14	0.1962
S4	6274.08	3805.79	101.78	37.45	51.84	90.54	7.26	0.2089
S5	5447.76	3296.12	82.06	30.04	42.00	72.77	5.78	0.2113
Base glass	6091.32	3738.36	89.05	33.54	44.33	80.35	6.75	0.1978

The mechanical properties of the synthesized glasses have also been investigated by applying the Makishima and Mackenzie model [72], depending on the chemical composition, packing density(V_t) and dissociation energy per unit volume $(G_t)$of the respective glasses. The mechanical properties such as Young's(E_m), bulk (k_m), shear(G_m), longitudinal (L_m) modulus, Poisson's ratio (υ), fractal bond connectivity (d_f), and hardness (H), according to the MM model were computed by using the formulas listed below and the corresponding mechanical properties of the glasses are shown in **Table 8**.

$$V_t = \left(\frac{1}{V_m}\right) \sum y_i V_i \quad (31)$$

$$V_i = N_A \left(\frac{4\pi}{3}\right) (xR_A^3 + yR_O^3) \quad (32)$$

Where, N_A and y_i denote Avogadro's number and mole fraction of component i, respectively, and R_A and R_O signify the Pauling ionic radii of cation and oxygen, respectively, in an oxide, A_xO_y system.

$$E_m = 2V_t G_t \quad (33)$$

$$k_m = 10V_t^2 G_t \quad (34)$$

$$G_m = \frac{30V_t^2 G_t}{(10.2V_t - 1)} \quad (35)$$

$$L_m = k_m + \left(\frac{4}{3}\right) G_m \quad (36)$$

$$\upsilon = 0.5 - \left(\frac{1}{7.2V_t}\right) \quad (37)$$

$$d_f = 4 \times \left(\frac{G_m}{k_m}\right) \quad (38)$$

$$H = \frac{(1-2\upsilon)E_m}{6(1+\upsilon)} \quad (39)$$

Table 8. Mechanical properties of the glasses according to the Makishima & Mackenzie model.

Samples	V_t	$G_t \times 10^6$ (kj/m^3)	E_m(Gpa)	k_m(Gpa)	G_m(Gpa)	L_m(Gpa)	υ	d_f	H (Gpa)
S1	0.5598	58.14	64.90	43.37	27.54	80.17	0.2518	2.54	4.2893
S2	0.5362	54.52	58.34	37.45	25.35	71.54	0.2409	2.70	4.0604
S3	0.5393	58.76	63.49	40.88	27.98	78.36	0.2424	2.74	4.3880
S4	0.5838	58.11	67.72	47.29	28.42	85.24	0.2621	2.40	4.2549
S5	0.4636	54.48	50.39	30.04	22.54	60.17	0.2000	3.00	4.1991
Base glass	0.5211	58.79	61.39	38.67	26.56	74.12	0.2334	2.75	4.4231

The all-similar mechanical parameters have been computed by the Rocherulle model also, where the packing density parameter in the Makishima and Mackenzie model has been informed as in Eq. (40), and (41), and shown in **Table 9**:

$$C_t = \sum_i y_i C_i \quad (40)$$

$$C_i = N_A \left(\frac{4\pi}{3V_m}\right)(xR_A^3 + yR_O^3) \quad (41)$$

Table 9. Mechanical properties of the glasses measured according to the Rocherulle model.

Samples	C_t	$G_t^* \times 10^6$ (kj/m^3)	E_m^* (Gpa)	k_m^*(Gpa)	G_m^*(Gpa)	L_m^*(Gpa)	υ^*	d_f^*	H^*(Gpa)
S1	0.5503	58.14	64.02	42.18	27.56	78.53	0.2476	2.61	4.317
S2	0.5404	54.52	58.93	38.15	25.36	72.04	0.2429	2.66	4.063
S3	0.5519	58.76	64.87	42.56	27.54	79.35	0.2483	2.59	4.360

S4	0.5502	58.11	63.86	42.05	27.34	78.64	0.2475	2.60	4.309
S5	0.5402	54.48	58.76	38.00	25.28	71.56	0.2428	2.66	4.053
Base glass	0.5521	58.79	64.84	42.56	27.64	79.56	0.2484	2.59	4.356

The fractal bond connectivity (d_f) represents structures of the studied glass samples which shows 3.00 to 2.40 [71]. The (d_f) value becomes 1, 2, 3 for chain, layer structure, and 3D networks of tetrahedral coordination polyhedral systems correspondingly. These obtained (d_f) values of the studied glass specimens are very similar to 3, implying a 3D layer glass network structure. The mechanical properties of the examined glass specimens are illustrated in **Fig. 16**, and the properties are reduced with the increase of PbO ($0 \leq x \leq 10$, x in mol%) concentrations in pure sodium silicate glass network structure, and the determined number of metallic oxides ($Cu_2O+CuO+SnO_2$) (<0.22mol%) added sodium silicate glass structure respectively. The properties in **Fig. 16** also show that the properties of the y(1) glass series are well improved than the properties of y(0) glass series due to the addition of metallic oxides ($Cu_2O+CuO+SnO_2$) (<0.22mol%) in the sodium silicate glass networks. Both glass series (y (1), and y(0)) are decreased with increasing concentrations of PbO ($0 \leq x \leq 10$, x in mol%) due to decrease packing density (V_t), and dissociation energy (G_t) of the examined glass specimens. The packing density (V_t) of the studied glass samples is reduced with increasing PbO mol% due to an increase in the studied glasses' molar volume (V_m) (cm^3). Similarly, since the bond force of Pb-O is lesser than of Si-O, the dissociation energy of the glasses lowered when the PbO (mol%) concentrations rose in the glass latticework. Hence, rigidity including total modulus of elasticity of the studied glass samples decrease with increasing PbO mol% due to reducing of (V_t), and (G_t) values, and subsequently due to the increase of molar volume (V_m) (cm^3) also.

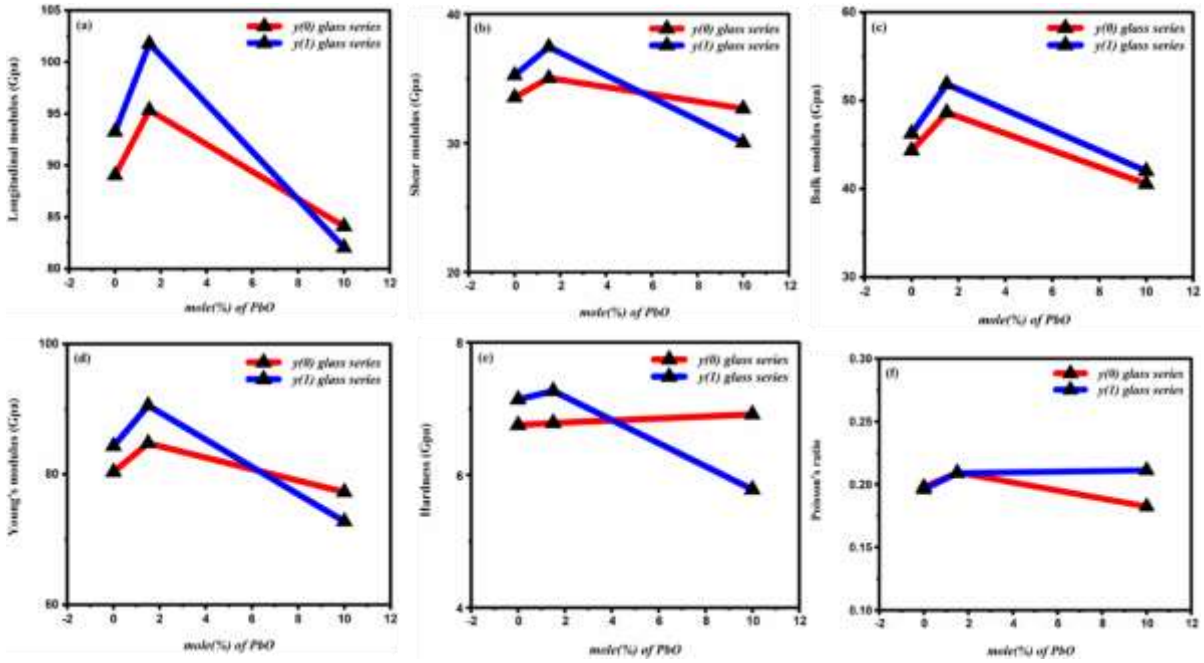

Fig. 16. Impact of mechanical characteristics with the addition of PbO ($0 \leq x \leq 10$, x in mol%) in the studied glass system {$xPbO\text{-}y(0.14Cu_2O\text{-}0.05CuO\text{-}0.03SnO_2)\text{-}30Na_2O\text{-}(70\text{-}0.22y\text{-}x)\ SiO_2$}.

4. Conclusions

Within the tenure of the research, two separate sodium silicate glass series first one (y(0)) doped only with PbO, and the second one (y(1)) doped with Cu_2O, CuO, SnO_2, and PbO with various ratio, have been synthesized successfully via melt annealing method. The X-ray diffraction analysis shows that non-crystallographic peaks are not detectable which is the confirmation of the amorphous nature of the samples. Reflection, transmission, and absorption studies of the respective specimens are accomplished by utilizing UV-Vis spectroscopy which also has been useful for computing the optical band gap energy of the specimens. Indirect energy gap (E_{gind}) of the studied samples is measured between 1.64 & 2.61 eV. The prepared glass series are found to be translucent until the addition of at max 10.22 mol% metallic oxides (Cu_2O+CuO+SnO_2+PbO) in sodium silicate glass networks makes the glasses opaque. The parameters $such\ as\ (R_{VIS}, T_{VIS}, A_{VIS})$ which are responsible for daylighting in the building, are found to be in the range of 32 to 40%, 27 to 40%, and 20 to 35% respectively in the studied samples, and the parameters $(R_{solar}, T_{solar}, A_{solar})$ which are key indicator of heat gain of the building, are noticed to be in the range of 28 to 41%,27 to 40%, 19 to 44%, respectively. It is also noticed that the addition of PbO ($0 \leq x \leq 10$, x in mol%), and metallic oxides (Cu_2O+CuO+SnO_2) (<0.22 mol%) in sodium silicate glass networks improves the refractive index (n), extinction coefficient (k), and complex dielectric constants $(\mathcal{E}_r, \mathcal{E}_i)$ of the synthesized specimen glasses. The large charge transfer UV absorption band exhibits around 316 nm for all the studied glass specimens, occurred due to the Pb^{2+} ions, and the existence of Fe^{3+} ions as an impurity. The average refractive index (n_0) via Tauc's method and the corresponding nonlinear refractive index (n_2) of each assessed glass specimen is found, where (n_0) values vary in the range of 2.51 to 2.91. Furthermore, oxygen packing density, optical basicity (Λ_{th}), molar refraction (R_m),polarizability (α_m), reflection loss (R_L), optical transmission (T), metallization criterion (M_c), optical electronegativity $(\Delta\chi^*)$, and third order nonlinear optical susceptibility $(\chi^{(3)})$ of examined glass specimens have been calculated. The findings of all characteristics demonstrate that the physical, and optical characteristics of all studied glasses are strongly connected to the addition of metallic oxides (Cu_2O+CuO+SnO_2) (<0.22 mol.%) and PbO mol.% concentrations. The elastic moduli, and rigidity of the xPbO-y(0.14Cu_2O-0.05CuO-0.03SnO_2)-30Na_2O-(70-0.22y-x) SiO_2 glass systems got reduced with the gradual incorporation of PbO concentrations. The reported mechanical properties decrease with increasing PbO concentrations in the glasses due to a decrease in packing density (V_t) , and dissociation energy (G_t) of the studied glasses. Raising metallic concentrations improves absorption, refractive index, and density, yet drastically diminishes, mechanical, and visible characteristics such as transparency, resulting in black darkened glasses that are unattractive. As such, the purpose of this study seems to figure out the suitable level of metals within sodium silicate glass structures resulting in outstanding dense optical glasses that have outstanding mechanical properties, refractive index, and transparency that could prove truly useful when employed as a construction material and optoelectronic implements in the not-too-distant future.

Acknowledgements

The author (Debajyoti Mahapatra) heartily acknowledges the Indian Institute of Technology (BHU), INDIA, and its Central Instrument Facility (CIF, IIT BHU) for the help they provided in accomplishing the research.

Efforts of the contributors

Debajyoti Mahapatra prepared the research review, executed the tests, assembled, and analysed the data,

and composed the initial article. Dr. Subrata Panda, and Dr. Preetam Singh coordinated the project and looked at including modified the draft, figures, document, and table document. Dr. Anil Kumar and, Dr. Subrata Panda organized materials, secured funds, and managed every aspect of the project.

Information Accessibility

Under an appropriate request, the associated contributor will supply the datasets employed or validated throughout the present research.

Declarations

Affirmation of morality: This is not applicable during this instance.
Consistency in involvement: This is not valid.
Publishing approval: The completed content had to be approved by all authors.
Disputes concerning competition: The authors assert that they have no opposing goals.
Declaration of funding: Inapplicable.

References

1. Kaur P, Singh D, Singh T. Heavy metal oxide glasses as gamma rays shielding material. Nuclear Engineering and Design. 2016 Oct 1;307:364-76. https://doi.org/10.1016/j.nucengdes.2016.07.029.
2. Singh GP, Kaur P, Kaur S, Arora D, Singh DP. Structural and Optical Investigation of Aluminium-Lithium-Borate Glasses. Asian Review of Mechanical Engineering. 2012 Jul;1(2):6.
3. Shrikhande VK. Preparation and characterization of special glasses for sealing and other applications. In IOP Conference Series: Materials Science and Engineering 2009 Jul 1 (Vol. 2, No. 1, p. 012016). IOP Publishing. 10.1088/1757-899X/2/1/012016.
4. Lancry M, Régnier E, Poumellec B. Fictive temperature in silica-based glasses and its application to optical fibre manufacturing. Progress in Materials Science. 2012 Jan 1;57(1):63-94.https://doi.org/10.1016/j.pmatsci.2011.05.002.
5. Kirankumar G, Shaik S, Setty AB. Thermal and energy saving analysis by using tinted double window glass combinations for heat gain in buildings. International Energy Journal. 2018 May 31;18(2).
6. Bäck LG, Ali S, Karlsson S, Wondraczek L, Jonson B. X-ray and UV-Vis-NIR absorption spectroscopy studies of the Cu (I) and Cu (II) coordination environments in mixed alkali-lime-silicate glasses. Journal of Non-Crystalline Solids: X. 2019 Sep 1; 3:100029.https://doi.org/10.1016/j.nocx.2019.100029.
7. Lakshminarayana G, Buddhudu S. Spectral analysis of Cu^{2+}: B_2O_3–ZnO–PbO glasses. Spectrochimica Acta Part A: Molecular and Biomolecular Spectroscopy. 2005 Nov 1;62(1-3):364-71.https://doi.org/10.1016/j.saa.2005.01.014.
8. Duran A, Fernandez Navarro JM. The colouring of glass by Cu^{2+} ions. Physics and chemistry of glasses. 1985;26(4):125-31.
9. Bamford CR. The application of the ligand field theory to coloured glasses. Phys. Chem. Glasses. 1962 Dec;3(6):189-202.
10. Kondo Y, Kuroiwa Y, Sugimoto N, Manabe T, Ito S, Tokizaki T, Nakamura A. Third-order optical non-linearities of CuCl-doped glasses in a near resonance region. Journal of non-crystalline solids. 1996(196):90-4.

11. Khan I, Rooh G, Rajaramakrishna R, Srisittipokakun N, Kim HJ, Kaewkhao J, Ruangtaweep Y. Photoluminescence Properties of Dy $^{3+}$ Ion-Doped Li_2O-PbO-Gd_2O_3-SiO_2 Glasses for White Light Application. Brazilian Journal of Physics. 2019 Oct 15; 49:60514.https://doi.org/10.1007/s13538-019-00695-0.
12. Khodadadi A, Taherian R. Investigation on the radiation shielding properties of lead silicate glasses modified by ZnO and BaO. Materials Chemistry and Physics. 2020 Sep 1; 251:123136.https://doi.org/10.1016/j.matchemphys.2020.123136.
13. Al-Hadeethi Y, Sayyed MI, Rammah YS. Fabrication, optical, structural and gamma radiation shielding characterizations of GeO2-PbO-Al2O3–CaO glasses. Ceramics International. 2020 Feb 1;46(2):2055-62.https://doi.org/10.1016/j.ceramint.2019.09.185.
14. Al-Buriahi MS, Rammah YS. Investigation of the physical properties and gamma-ray shielding capability of borate glasses containing PbO, Al2O 3 and Na2O. Applied Physics A. 2019 Oct;125:1-8.https://doi.org/10.1007/s00339-019-3020-z.
15. Lakshminarayana G, Buddhudu S. Spectral analysis of Eu^{3+} and Tb^{3+}: B_2O_3–ZnO–PbO glasses. Materials Chemistry and Physics. 2007 Apr 15;102(2-3):181-6.https://doi.org/10.1016/j.matchemphys.2006.11.020.
16. Gowda VV, Reddy CN, Radha KC, Anavekar RV, Etourneau J, Rao KJ. Structural investigations of sodium diborate glasses containing PbO, Bi_2O_3 and TeO_2: Elastic property measurements and spectroscopic studies. Journal of Non-Crystalline Solids. 2007 May 1;353(11-12):1150-63.https://doi.org/10.1016/j.jnoncrysol.2006.12.117.
17. Lakshminarayana G, Sagar RV, Buddhudu S. Emission analysis of Dy^{3+} and Pr^{3+}: Bi_2O_3–ZnF_2–B_2O_3–Li_2O–Na_2O glasses. Physica B: Condensed Matter. 2008 Jan 1;403(1):81-6.https://doi.org/10.1016/j.physb.2007.08.010.
18. Takaishi T, Jin J, Uchino T, Yoko T. Structural study of PbO–B_2O_3 glasses by X-ray diffraction and 11B MAS NMR techniques. Journal of the American Ceramic Society. 2000 Oct;83(10):2543-8.https://doi.org/10.1111/j.1151-2916.2000.tb01588.x.
19. Shrikhande VK. Preparation and characterization of special glasses for sealing and other applications. In IOP Conference Series: Materials Science and Engineering 2009 Jul 1 (Vol. 2, No. 1, p. 012016). IOP Publishing. 10.1088/1757-899X/2/1/012016.
20. Osipov AA, Osipova LM, Hruška B, Osipov AA, Liška M. FTIR and Raman spectroscopy studies of ZnO-doped BaO· $2B_2O_3$ glass matrix. Vibrational Spectroscopy. 2019 Jul 1; 103:102921.https://doi.org/10.1016/j.vibspec.2019.05.003.
21. Sun H, Wen L, Xu S, Dai S, Hu L, Jiang Z. Novel lithium–barium–lead–bismuth glasses. Materials Letters. 2005 Apr 1;59(8-9):959-62.https://doi.org/10.1016/j.matlet.2004.09.051.
22. Abo-Naf SM, Elwan RL, Marzouk MA. Structure–property correlations in the SiO_2–PbO–Bi_2O_3 glasses. Journal of Materials Science: Materials in Electronics. 2012 May; 23:1022-30.https://doi.org/10.1007/s10854-011-0541-4.
23. Worrell CA, Henshall T. Vibrational spectroscopic studies of some lead silicate glass. Journal of Non-Crystalline Solids. 1978 Sep 1;29(3):283-99.https://doi.org/10.1016/0022-3093(78)90150-3.
24. Fayon F, Bessada C, Massiot D, Farnan I, Coutures JP. 29Si and 207Pb NMR study of local order in lead silicate glasses. Journal of Non-Crystalline Solids. 1998 Jul 11; 232:403-8.https://doi.org/10.1016/S0022-3093(98)00470-0.

25. Rabinovich EM. Lead in glasses. Journal of Materials Science. 1976 May; 11:925-48.https://doi.org/10.1007/BF00542311.
26. LEVENTHA. M, Bray PJ. Nuclear magnetic resonance investigations of compounds and glasses in systems PbO-B2O3 and PbO-SiO2. Physics and chemistry of glasses. 1965 Jan 1;6(4):113.
27. Dupree R, Ford N, Holland D. Examination of the/sup 29/Si environment in the PbO-SiO/sub-2/system by magic angle spinning nuclear magnetic resonance. Pt. 1. Glasses. Phys. Chem. Glasses;(United Kingdom). 1987 Apr 1;28(2).
28. Zahra AM, Zahra CY, Piriou B. DSC and Raman studies of lead borate and lead silicate glasses. Journal of non-crystalline solids. 1993 Mar 1;155(1):45-55.https://doi.org/10.1016/0022-3093(93)90470-I.
29. Liu L. Infrared spectroscopy on lead silicate glass. Zeitschrift für Physik B Condensed Matter. 1993 Dec;90(4):393-9.https://doi.org/10.1007/BF01308818.
30. Kabanov VO, Podol'skaya TM, Yanush OV. Raman spectra and structure of the PbO-SiO2 glasses. Glass Physics and Chemistry. 1996;22(1):19-26.
31. Wang PW, Zhang L. Structural role of lead in lead silicate glasses derived from XPS spectra. Journal of non-crystalline solids. 1996 Jan 1;194(1-2):129-34. https://doi.org/10.1016/0022-3093(95)00471-8.
32. Al-Buriahi MS, Rammah YS. Investigation of the physical properties and gamma-ray shielding capability of borate glasses containing PbO, Al_2O_3 and Na_2O. Applied Physics A. 2019 Oct;125:1-8. https://doi.org/10.1007/s00339-019-3020-z.
33. Doweidar H, Moustafa YM, El-Egili K, Abbas I. Infrared spectra of Fe2O3–PbO–P2O5 glasses. Vibrational spectroscopy. 2005 Jan 14;37(1):91-6.https://doi.org/10.1016/j.vibspec.2004.07.002.
34. Kaur R, Singh S, Pandey OP. Structural variation in gamma-ray irradiated PbO–Na_2O–B_2O_3–SiO_2 glasses. Solid State Communications. 2014 Jun 1; 188:40-4.https://doi.org/10.1016/j.ssc.2014.02.022.
35. Alothman MA, Kurtulus R, Olarinoye IO, Kavas T, Mutuwong C, Al-Buriahi MS. Optical, elastic, and radiation shielding properties of Bi_2O_3-PbO-B_2O_3 glass system: a role of SnO_2 addition. Optik. 2021 Dec 1; 248:168047.https://doi.org/10.1016/j.ijleo.2021.168047.
36. Goswami M, Sudarsan V, Shrikhande VK, Kothiyal GP, Kulshreshtha SK. Structural and Thermophysical Properties of $(PbO)_{0.5}(SiO_2)_{0.5}$ Glasses: Effect of SnO_2 Incorporation. Journal of the American Ceramic Society. 2008 Mar;91(3):986-9.https://doi.org/10.1111/j.1551-2916.2007.02209.x.
37. Chen Q, Su K, Wang H, Chen Q. SnO_2 modified thermal, mechanical and magneto-optical property improvement of PbO-Bi_2O_3-B_2O_3 glass. Journal of Non-Crystalline Solids. 2018 Aug 1; 493:20-8.https://doi.org/10.1016/j.jnoncrysol.2018.04.035.
38. Ziemath EC, Saggioro BZ, Fossa JS. Physical properties of silicate glasses doped with SnO_2. Journal of non-crystalline Solids. 2005 Dec 15;351(52-54):3870-8.https://doi.org/10.1016/j.jnoncrysol.2005.10.016.
39. Kuz'menkova NM, Bobkova NM. The phase composition of glass ceramics of the system K_2O–Li_2O–Al_2O_3–SiO_2–SnO_2–ZrO_2 for metal-ceramic coatings. Glass and Ceramics. 2010 Nov; 67:187-9.https://doi.org/10.1007/s10717-010-9259-7.
40. Goyal P, Sharma YK, Pal S, Bind UC, Huang SC, Chung SL. Structural, optical and physical analysis of B_2O_3–SiO_2–Na_2O–PbO–ZnO glass with Sm^{3+} ions for reddish–orange laser emission. Journal of Luminescence. 2017 Dec 1; 192:1227-34.https://doi.org/10.1016/j.jlumin.2017.08.061.

41. Mecherikunnel AT, Richmond J. Spectral distribution of solar radiation. 1980 Sep 1.
42. Torres-Carrasco M, Palomo A, Puertas F. Sodium silicate solutions from the dissolution of glass wastes. Statistical analysis. http://dx.doi.org/10.3989/mc.2014.05213.
43. Shaaban KS, Abd-Allah WM, Saddeek YB. Gamma rays' interactions with CdO-doped lead silicate glasses. Optical and Quantum Electronics. 2020 Jan; 52:1-7.https://doi.org/10.1007/s11082-019-2094-3.
44. He X, Shen X, Huang Q, Zhang J, He Y, Liu T, Lu A. Study on the structure, fining and properties of non-alkali aluminoborosilicate glasses containing SnO_2. Journal of Non-Crystalline Solids. 2021 May 1; 559:120670.https://doi.org/10.1016/j.jnoncrysol.2021.120670.
45. MacDonald SA, Schardt CR, Masiello DJ, Simmons JH. Dispersion analysis of FTIR reflection measurements in silicate glasses. Journal of non-crystalline solids. 2000 Sep 1;275(1-2):72-82.https://doi.org/10.1016/S0022-3093(00)00121-6.
46. Kaur R, Singh S, Pandey OP. Structural variation in gamma-ray irradiated PbO–Na_2O–B_2O_3–SiO_2 glasses. Solid State Communications. 2014 Jun 1; 188:40-4.https://doi.org/10.1016/j.ssc.2014.02.022.
47. Abdelghany AM, ElBatal FH, ElBatal HA, EzzElDin FM. Optical and FTIR structural studies of CoO-doped sodium borate, sodium silicate and sodium phosphate glasses and effects of gamma irradiation-a comparative study. Journal of Molecular Structure. 2014 Sep 25; 1074:503-10.https://doi.org/10.1016/j.molstruc.2014.06.011.
48. Ibrahim MM, A. Fanny M, Hassaan MY, ElBatal HA. Optical, FTIR and DC conductivity of soda lime silicate glass containing cement dust and transition metal ions. Silicon. 2016 Jul; 8:443-53. https://doi.org/10.1007/s12633-015-9362-z.
49. Gorantla KK, Shaik S, Setty AB. Daylighting and thermal analysis using various double reflective window glasses for green energy buildings. Journal homepage: http://iieta. org/Journals/IJHT. 2018 Sep 1;36(3):1121-9.http://iieta.org/Journals/IJHT.
50. Abdelghany AM, El-Damrawi G, Oraby AH, Madshal MA. Optical and FTIR structural studies on CoO-doped strontium phosphate glasses. Journal of Non-Crystalline Solids. 2018 Nov 1; 499:153-8.https://doi.org/10.1016/j.jnoncrysol.2018.07.022.
51. Nahrawy AE, Moez AA, Saad AM. Sol-gel preparation and spectroscopic properties of modified sodium silicate/tartrazine dye nanocomposite. Silicon. 2018 Sep;10:2117-22.https://doi.org/10.1007/s12633-017-9740-9.
52. Al-Hadeethi Y, Sayyed MI, Rammah YS. Fabrication, optical, structural and gamma radiation shielding characterizations of GeO_2-PbO-Al_2O_3–CaO glasses. Ceramics International. 2020 Feb 1;46(2):2055-62.https://doi.org/10.1016/j.ceramint.2019.09.185.
53. Al-Buriahi MS, Rammah YS. Radiation sensing properties of tellurite glasses belonging to ZnO–TeO_2–PbO system using Geant4 code. Radiation Physics and Chemistry. 2020 May 1; 170:108632.https://doi.org/10.1016/j.radphyschem.2019.108632.
54. Volotinen TT, Parker JM, Bingham PA. Concentrations, and site partitioning of Fe2+ and Fe3+ ions in a soda–lime–silica glass obtained by optical absorbance spectroscopy. Physics and Chemistry of Glasses-European Journal of Glass Science and Technology Part B. 2008 Oct 15;49(5):258-70.
55. Johnston WD, Chelko A. Oxidation-Reduction Equilibria in Molten Na_2O. $2SiO_2$ Glass in Contact with Metallic Copper and Silver. Journal of the American Ceramic Society. 1966 Oct;49(10):562-4. https://doi.org/10.1111/j.1151-2916.1966.tb13163.x.

56. Banerjee S, Paul A. Thermodynamics of the System Cu-O and Ruby Formation in Borate Glass. Journal of the American Ceramic Society. 1974 Jul;57(7):286-90.https://doi.org/10.1111/j.1151-2916.1974.tb10902.x.
57. Dwivedi RN, Nath P. Mechanism of Red Colour Formation in Photosensitive and Normal Copper-Ruby Glasses. Transactions of the Indian Ceramic Society. 1980 Jan 1;39(1):23-8.https://doi.org/10.1080/0371750X.1980.10840717.
58. Singh SP, Prasad G, Nath P. Kinetic Study of Cu^{+}-Cu^{2+} Equilibrium in Sodium Na_2O–Al_2O_3–B_2O_3 Glass. Journal of the American Ceramic Society. 1978 Sep;61(9-10):377-9.https://doi.org/10.1111/j.1151-2916.1978.tb09340.x.
59. Weyl WA. Coloured Glasses, Society of Glass Technology. Sheffield, UK. 1951;329.
60. Singh SP, Prasad G, Nath P. Absorption characteristics of cupric ion in sodium aluminoborate glass. Bull. Cent. Glass Ceram. Res. Inst. Calcutta. 1978;25(2):38-42.
61. Kumar S, Nag BB. Electrical Properties of Crystallized Glasses in the System MgO-Al_2O_3-SiO_2-TiO_2. Journal of the American Ceramic Society. 1966 Jan;49(1):10-4.
62. Bamford CR. The application of the ligand field theory to coloured glasses. Phys. Chem. Glasses. 1962 Dec;3(6):189-202.
63. Bates T, Mackenzie JD. Modern aspects of the vitreous state. Butterworth, London. 1962.
64. Singh SP, Kumar A. Molar extinction coefficients of the cupric ion in silicate glasses. Journal of materials science. 1995 Jun;30(11):2999-3004.https://doi.org/10.1007/BF00349674.
65. Khalil EM, El-Batal FH, Hamdy YM, Zidan HM, Aziz MS, Abdelghany AM. UV-visible and IR spectroscopic studies of gamma irradiated transition metal doped lead silicate glasses. Silicon. 2010 Jan;2:49-60. https://doi.org/10.1007/s12633-009-9029-8.
66. Marzouk SY, Seoudi R, Said DA, Mabrouk MS. Linear and non-linear optics and FTIR characteristics of borosilicate glasses doped with gadolinium ions. Optical Materials. 2013 Oct 1;35(12):2077-84. https://doi.org/10.1016/j.optmat.2013.05.023.
67. Lakshminarayana G, Buddhudu S. Spectral analysis of Cu^{2+}: B_2O_3–ZnO–PbO glasses. Spectrochimica Acta Part A: Molecular and Biomolecular Spectroscopy. 2005 Nov 1;62(1-3):364-71.https://doi.org/10.1016/j.saa.2005.01.014.
68. Dimitrov V, Komatsu T. An interpretation of optical properties of oxides and oxide glasses in terms of the electronic ion polarizability and average single bond strength. J. Univ. Chem. Technol. Metall. 2010 Feb;45(3):219-50.
69. Hammad AH, Elsaghier HM, Abbas W, Zidan NA, Marzouk SY. Investigation of some structural and optical properties of lithium sodium fluoroborate glasses containing cuprous oxide. Measurement. 2018 Feb 1; 116:170-7. https://doi.org/10.1016/j.measurement.2017.11.012.
70. Pauling L. The Nature of The Chemical Bond Third Edition 3rd.
71. Issa SA, Saddeek YB, Tekin HO, Sayyed MI, saber Shaaban K. Investigations of radiation shielding using Monte Carlo method and elastic properties of PbO-SiO_2-B_2O_3-Na_2O glasses. Current Applied Physics. 2018 Jun 1;18(6):717-27.https://doi.org/10.1016/j.cap.2018.02.018.
72. Inaba S, Fujino S, Morinaga K. Young's modulus and compositional parameters of oxide glasses. Journal of the American Ceramic Society. 1999 Dec;82(12):3501-7.https://doi.org/10.1111/j.1151-2916.1999.tb02272.x.